

**The influence of bulk rock MnO on garnet development in
metamorphic rocks of andalusite-staurolite grade;
Kanmantoo, South Australia.**

By

Wade J. Bollenhagen

This thesis is submitted as partial fulfillment for the
Honours degree of Bachelor of Science .

Department of Geology and Geophysics
University of Adelaide
November 1993

National Grid Reference (SI-54) 6627-I
6727-IV 1:50000

ABSTRACT

An outcrop of meta-pelitic schist from near the township of Kanmantoo, South Australia, was chosen to demonstrate the effect that increased bulk MnO content has on metamorphic assemblage development.

From bulk composition and petrological analyses it is observed that the presence of small amounts of MnO in high X_{Fe} pelitic rocks correspond with the development of garnet. The incorporation of Mn into the KFMASH model system describes the existence of garnet with andalusite and staurolite that KFMASH does not predict.

Furthermore it shown that modal abundances of garnet are proportional to bulk MnO rock contents, enhancing the prediction that MnO causes an expansion of all garnet-bearing assemblages. This allows for the description of the numerous appearances of the garnet mineral in rocks that have calculated temperatures and pressures, for which it is not predicted to exist at.

ACKNOWLEDGEMENTS

Firstly, I would like to thank my supervisor Dr. Mike Sandiford, who gave me the opportunity to experience a wonderful and thought provoking year. For without this opportunity my life would have been very different.

The greatest appreciation must go to my family, for without them and their support this year would not have been possible. I hope that I do not dissappoint you, as you have made me so proud for the faith you had placed in me.

To all the technical staff in the Geology department, thank you, your time and assistance was and is invaluable to myself and many others. Thanks to Hue Rosser and the staff at C.E.M.M.S.A. for your assistance during the "sessions".

Thanks to Kurt Stuwe, Karin Ehlers, Jo Arnold and Ian Scrimgeour for your countless contributions towards the completion of this thesis, particularly Kurt who`s time and suggestions I have found extremely valuable.

Last, but by no means least, to all my friends (of which the list appears endless), thank you for everything, whilst we travelled along this hellish path. To my friends Chris, John C, Scott, Bruce, Paul and Mary J., it was a long way but we made it.

CHAPTER 1. Introduction.....	1
CHAPTER 2. Geology of the KANMANTOO Area.....	3
2.1. Geological Background.....	3
2.2. Metasediments of the Kanmantoo Area.....	3
2.2.1. Structure.....	4
2.2.2. Metamorphic considerations for the Kanmantoo.....	4
2.3. KFMASH Model Predictions for mineral assemblages.....	5
CHAPTER 3. Mineral Assemblages and Bulk Compositions of Meta- pelitic Rocks of Kanmantoo, South Australia.	
3.1. Introduction.....	7
3.2. Bulk Composition of sample space.....	8
3.2.1. Variations in the sample space.....	8
3.2.2. Composition Variation within the Assemblages.....	12
3.3. Mineral Chemistry	
3.3.1. Mineral Variations across the sample space.....	13
3.3.2. MnO partitioning amongst minerals.....	18
3.4. Comparison of mineral assemblages and bulk composition.....	19
3.4.1. Discussion of data.....	19
3.4.2. Conclusion.....	22
CHAPTER 4. Distribution of MnO in garnet across the sample space	
4.1. Andalusite-staurolite assemblage.....	23
4.2. Andalusite-staurolite-garnet assemblage.....	23
4.3. Staurolite-garnet assemblage.....	26
4.4. Summary.....	32
CONCLUSIONS.....	33

ACKNOWLEDGEMENTS

REFERENCES

APPENDICES

A - MAPS TO LOCALITIES

B - PETROLOGICAL ANALYSES

C - PROBE ANALYSES

D - BULK COMPOSITIONAL ANALYSES

LIST OF FIGURES

Figure 1:-Southern Adelaide Fold Belt

Figure 2:-Metamorphic Grades of Southern Adelaide Fold Belt, plus locality of field site

Figure3:-Kanamntoo Syncline

Figure4:-P-T pseudo-section

Figure5:-P-T pseudo-section

Figure6:- X_{Fe} of sample space

Figure7:- X_{Mn} of sample space

Figure8:- X_{Al} of sample space

Figure9:- X_{Mg} of sample space

Figure10:- X_{Mn} vs $Fe/Fe + Mg$

Figure11:-T- X_{Fe} diagram

Figure12:-AFM diagrams

Figure13:-AFMn diagrams

LIST OF GRAPHS

Graph 1a:-Distribution of garnet across sample space

Graph 2a:-Distribution of andalusite across sample space

Graph 3a:-Distribution of staurolite across sample space

Graph 2:- Comparison of garnet and bulk MnO content

Graph 3:- Distribution of MnO (in garnets) across sample space

Graph 4a:- MnO profile across garnet

Graph 4b:- MnO profile across garnet

Graph 4c:- MnO profile across garnet

Graph 4d:- MnO profile across garnet

Graph 4e:- MnO profile across garnet

Graph 4f:- MnO profile across garnet

Graph 4g:- MnO profile across garnet

Graph 4h:- MnO profile across garnet

Graph 4i:- MnO profile across garnet

Graph 4j:- MnO profile across garnet

Graph 4k:- MnO profile across garnet

Graph 4l:- MnO profile across garnet

LIST OF TABLES

Table 1:-Bulk composition of samples

Table 2:-Modal proportions

Table 3:-Mineral formulas

CHAPTER 1

INTRODUCTION

The analysis of metamorphic mineral assemblages is made simpler by the use of model systems. For example, pelitic rocks are often described in the model system K_2O , FeO , MgO , Al_2O_3 , SiO_2 and H_2O (KFMASH). Models are used to describe metamorphic rocks for two reasons; firstly, thermodynamic data is limited and not available for many trace element and minor components and secondly, to reduce the overall complexity of the systems being studied. For pelitic rocks, the model system (KFMASH) encompasses >95% of the rock forming components and is therefore generally considered as sufficient for describing their occurrence.

Importantly model systems have to be tested for their "appropriateness", and this is performed through the comparison of the predicted phase relations with natural rock assemblages. Failure of these models to account for natural metamorphic assemblages can be attributed to the influence of components neglected in the model design.

Dymoke and Sandiford (1992) have shown that the model KFMASH system accounts for many of the observed mineral associations in pelitic schists of the Mount Lofty Ranges, South Australia. However, this system fails to account for occurrence of garnet with andalusite and staurolite (+biotite+quartz+muscovite+ H_2O) that are seen in rocks of the Southern Adelaide Fold Belt (Mount Lofty Ranges).

The aim of this thesis is to examine the influence of the minor "neglected" components on mineral development, such as MnO on the stability of garnet in pelitic rocks during regional metamorphism. Principally rocks that exist close together experience identical pressures and temperatures so bulk composition can be considered to be the only variable factor influencing the development of mineral assemblages. To do this a small section of rock of greenschist grade was sampled from a locality near Kanmantoo, South Australia.

Three mineral assemblages exist in the sampled space, they are;

staurolite+garnet (+biotite+muscovite+quartz+H₂O)

andalusite+staurolite (+biotite+muscovite+quartz+H₂O)

andalusite+staurolite+garnet (+biotite+muscovite+quartz+H₂O)

The spatial relationship and modal abundances of the minerals in the above assemblages provide a basis for the consideration of bulk composition influence on their formation.

Bulk composition proportions of samples are compared to the modal abundance of minerals. It will be shown that MnO is preferentially partitioned into the garnet phase (Howell, 1991) and the development of garnet correlates with variations in bulk rock MnO content.

CHAPTER 2

GEOLOGY OF THE KANMANTOO AREA

2.1. Geological Background

The Kanmantoo Group metasediments form part of the Southern Adelaide Fold Belt (figure 1.), which comprises Neoproterozoic to early Palaeozoic sedimentary rocks that were deformed and metamorphosed during the Cambro-Ordovician Delamerian Orogeny, (Mancktelow, 1990; Jenkins, 1990). Overall the metamorphic grade of the belt is low (green schist facies), however the metamorphic grade increases substantially towards the east (Dymoke and Sandiford, 1992), see figure 2. This zonation correlates with the roughly linear NNW-SSE trending outcrops of felsic intrusives between Murray Bridge and Angaston. The heat dissipated from the intrusions is responsible for the development of biotite, andalusite-staurolite, fibrolite, prismatic sillimanite and migmatite zones that are observed in the Mount Lofty Ranges, (Dymoke and Sandiford, 1992).

2.2. Metasediments of the Kanmantoo Area

The field area (Map 1, contained in Appendix A) occupies an area of 20 km² West of the township of Kanmantoo which is located approximately 20km WNW of Murray Bridge, South Australia. Descriptions of lithology and structural relationships have been performed by others for the Kanmantoo area, Fleming (1971); Linqvist (1969); Mancktelow (1979); Marlow and Etheridge (1977). What is presented is a simplified view of field observations, concentrating on the implications for mineral development.

The field area provides a composition contrast between the pelitic units and the quartz rich units of the Brukunga Formation (after Miriams, 1969), in which outcrops of the Paringa Andalusite Horizons (after Miriams, 1969) occur, see Map 1, Appendix A. Outcrops of varying proportions of biotite, muscovite and quartz-rich units, inter-finger with the andalusite and staurolite bearing schists. Poor outcrop coupled with complex microstructure and composition variations makes any correlation between individual outcrops over a large scale difficult. Thus allowing each of the outcrops to be treated as a separate equilibrium assemblage, defined by their own P, T and X.

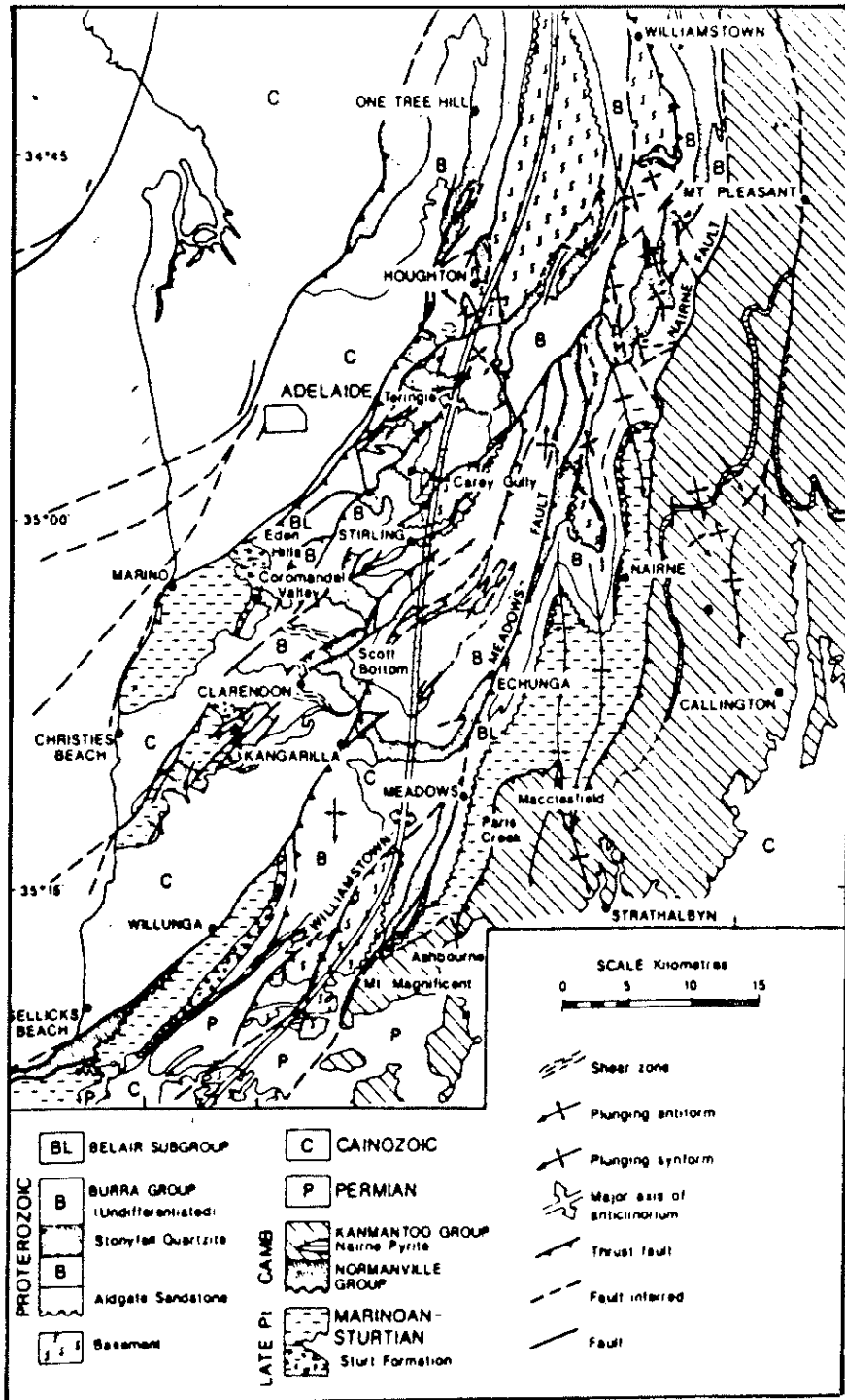


Figure 1 Geology of the Southern Adelaide Fold Belt, after Jenkins and Sandiford (1990).

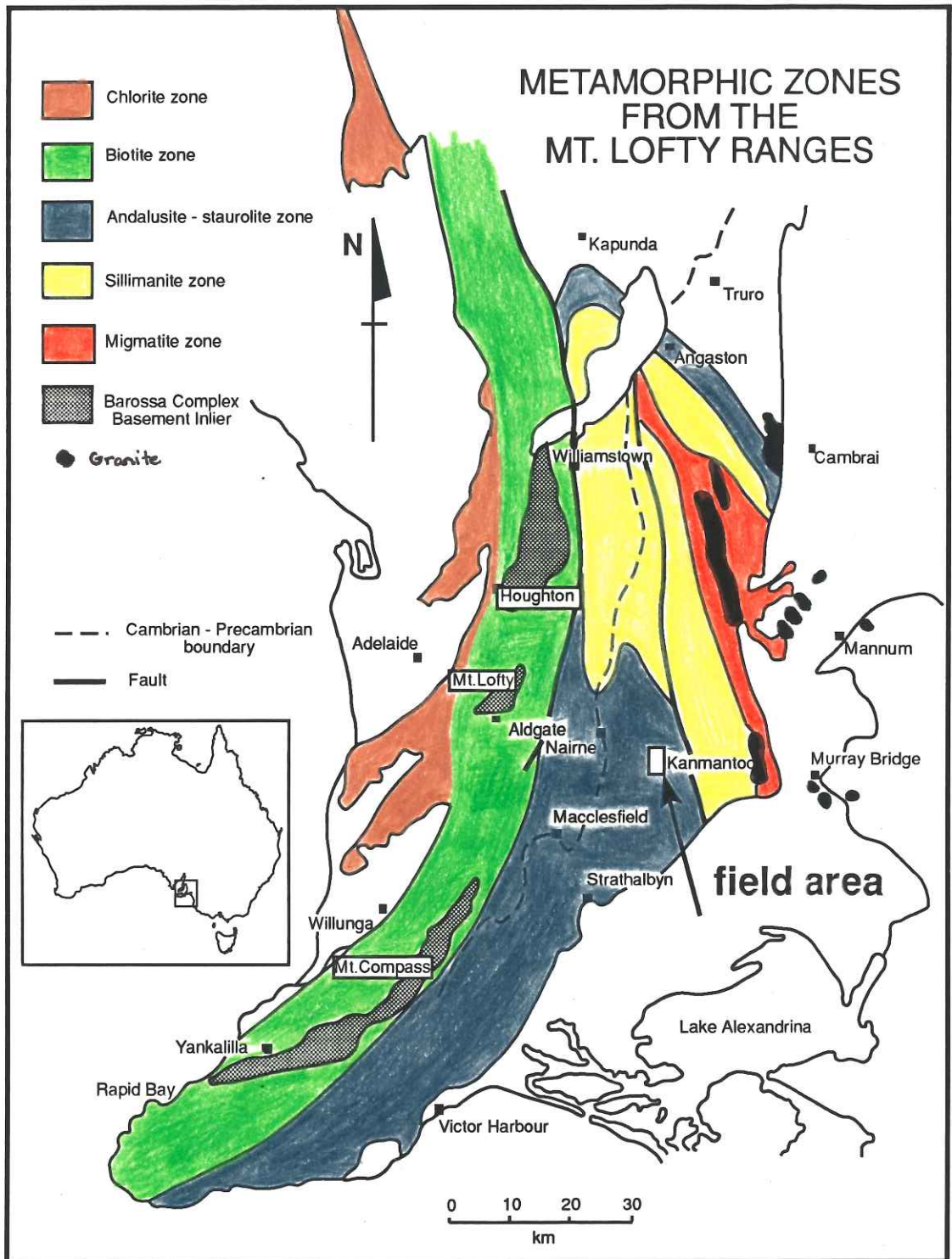


Figure 2

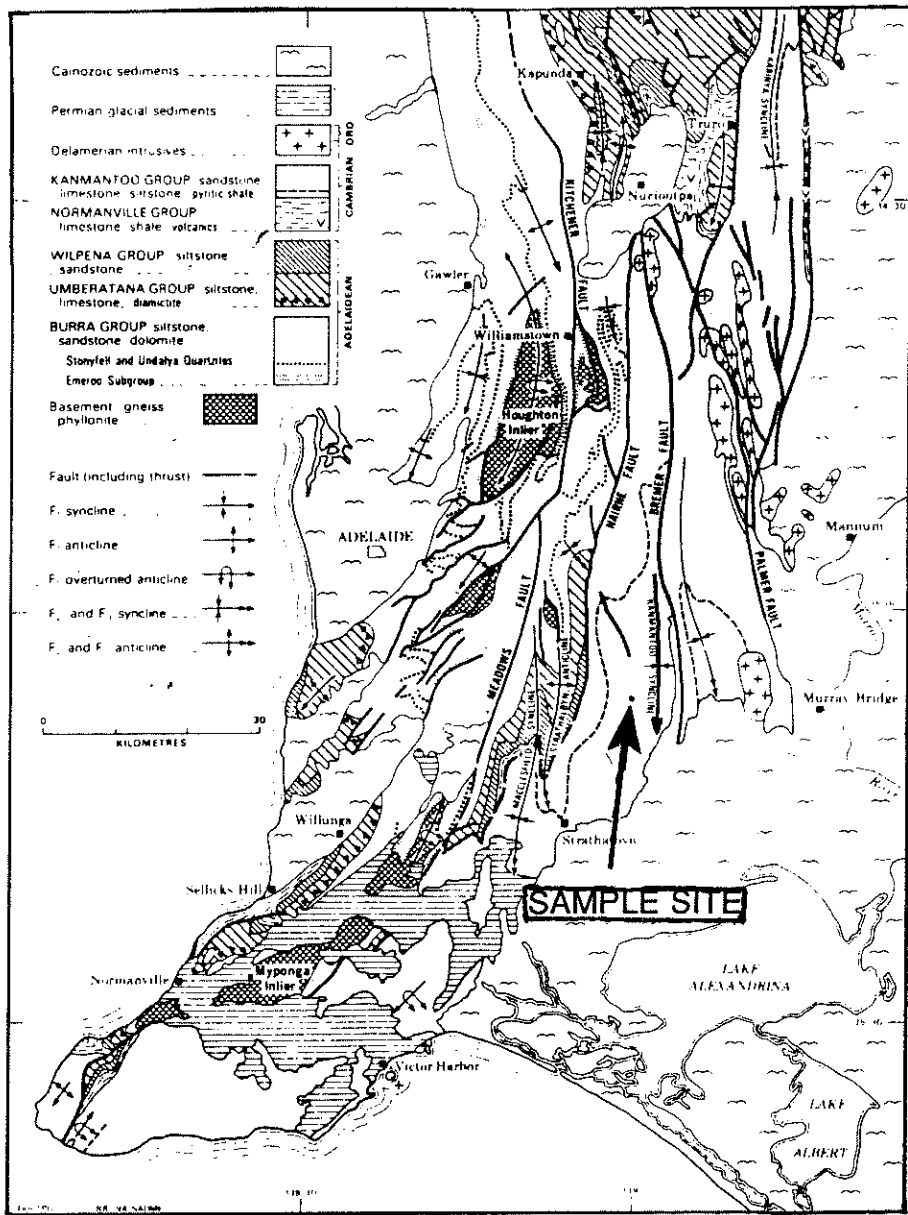


Figure 3 Geology of Kanmantoo area, showing the Kanmantoo syncline and field site, after Pries (1990).

2.2.1. Structure

The site of investigation lies within the Kanmantoo Syncline (see figure 3), which is one of a set of major folds which plunge South with fold axes plunging shallowly South. The macroscopic structure of the area appears very simple with an S_1 cleavage (010 east) dominating the nature of the rocks, overprinted by a later stage (D_2) more steeply dipping crenulation cleavage (S_2), parallel to S_1 . However very complex inclusion trail geometries in poikiloblasts indicate a complex microstructural evolution involving repeated crenulation of the fabric. This is an indication of a complex macroscopic history.

2.2.2. Metamorphic considerations for the Kanmantoo

The Kanmantoo Group sediments have undergone extensive metamorphism in the Cambro-Ordovician Delamerian Orogeny, (Fleming; 1971, Jenkins; 1990, Mancktelow; 1979). Intrusions located at Murray Bridge and Palmer are the probable source for the heat supply for metamorphism in the Kanmantoo Area during the deformation period.

Mineral assemblages outlined in the introduction were derived from petrological analyses of thin sections, (Appendix B). Inclusion patterns contained within andalusite, staurolite and garnet show continual mineral development with deformation. The peak of metamorphism is related to the second phase of deformation (D_2) (Dymoke and Sandiford (1992), this is seen where inclusion patterns of andalusite porphyroblasts mimic the S_2 crenulation in thin section.

Mapping in the Kanmantoo area (Map 1, Appendix A) has revealed rocks that are not described by the KFMASH system of Dymoke and Sandiford (1992) for "Buchan Style" metamorphism. Rocks are found to have assemblages containing the minerals garnet-andalusite-staurolite in close proximity with garnet "free" assemblages. These relationships provide the necessary assemblage relationships needed to demonstrate the influence of non-KFMASH components on mineral development.

2.3 KFMASH Model Predictions for mineral assemblages

Dymoke and Sandiford (1992) present calculated P-T pseudo-sections (Figures 4 and 5) and T- X_{Fe} diagrams (Fig. 11, section 3.4) for the KFMASH system, assuming an $a(H_2O) \approx 1$. These pseudo-sections of P-T and T- X_{Fe} were constructed for the assemblage chlorite, aluminosilicate, staurolite, cordierite, and/or garnet, with biotite+muscovite+quartz+ H_2O in excess in the KFMASH system. The pseudo-sections were generated with the internally consistent data set of Holland and Powell (1990) and version 2b.1. of the computer program Thermocalc.

Mineral abbreviations used in figures

and	andalusite	mu	muscovite
gt	garnet	q	quartz
st	staurolite	als	Al_2SiO_5 phase
bi	biotite	chl	chlorite
cd	cordierite	sill	sillimanite

The P-T pseudo-sections that were created for $X_{Fe}=0.7$ and $X_{Fe}=0.8$ are based upon the calculated P-T grid of Fig 2, Dymoke and Sandiford; (1992). The P-T pseudo-section calculated at $X_{Fe}=0.7$ predict that assemblages containing garnet and staurolite occur above P 5kb and T 575° C, above the andalusite "out" field, figure 4. It also predicts that the divariant assemblage containing staurolite and andalusite exists over a temperature range of 565-595° C, at pressures 4.0-4.25 kb. This prediction implies that assemblages containing garnet must occur at much higher P and T than those devoid of garnet.

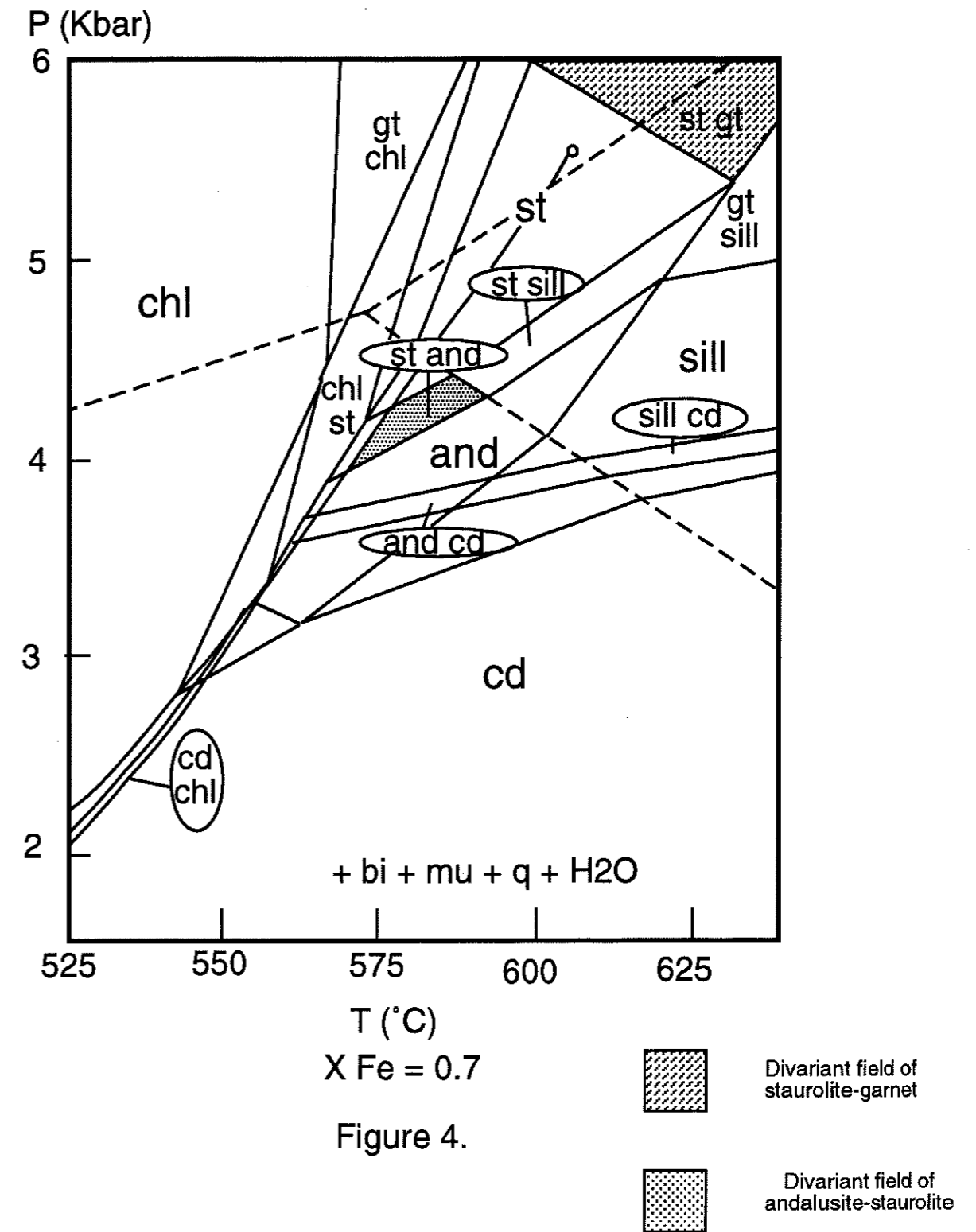
The pseudo-section calculated for $X_{Fe}=0.8$ shows changes in the predictions of the assemblage fields, in response to an increase in X_{Fe} . The predicted field of staurolite and garnet has a lower P and T than that of $X_{Fe}=0.7$, where the lowest P of formation is 4.75kb and lowest T of formation 560° C. These P and T are still above the andalusite "out" field, implying that the phase andalusite would not be seen in rocks at these conditions.

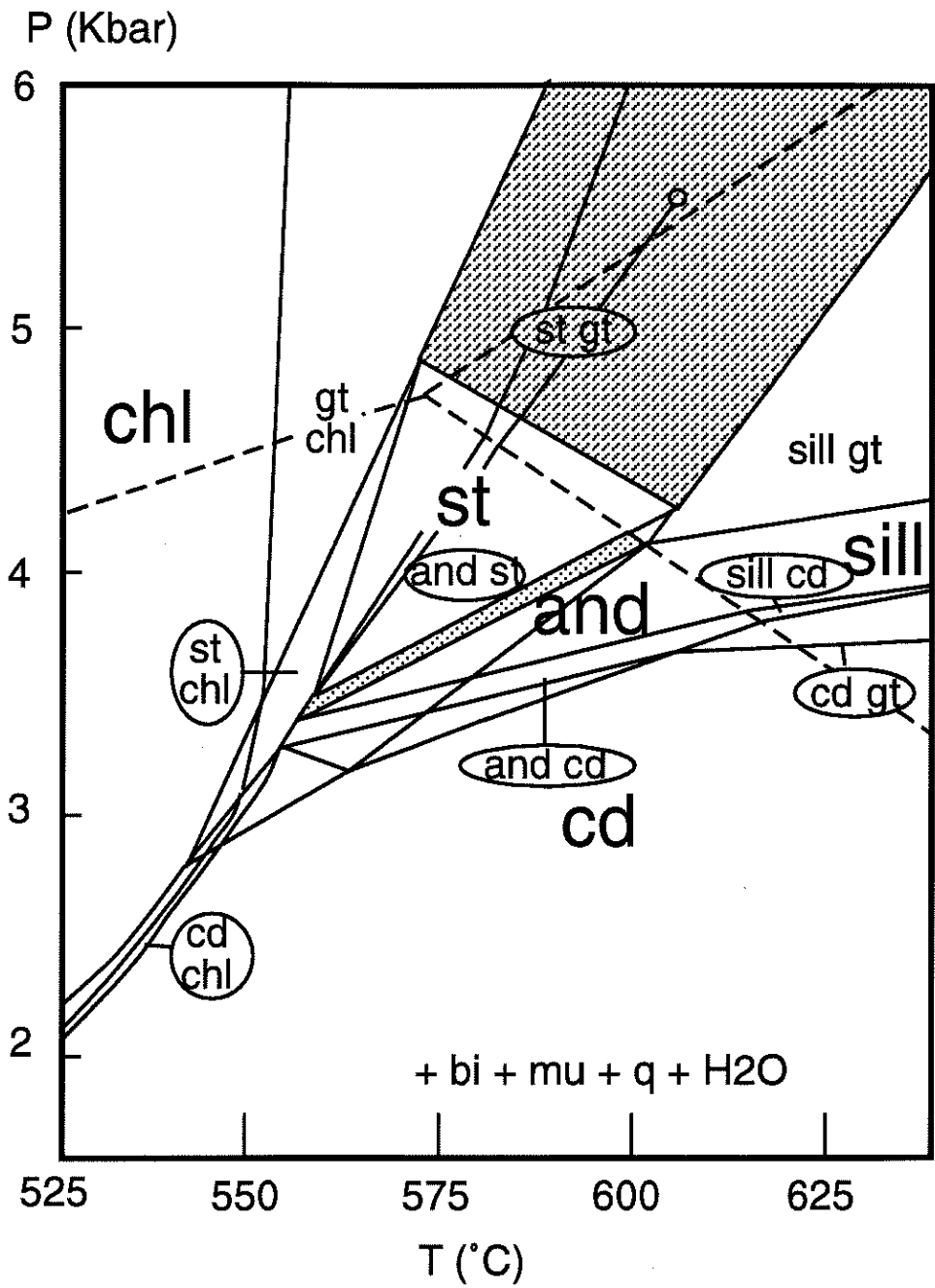
Figures 4 and 5 (next page)

Calculated P-T pseudo-sections at constant T- X_{Fe} for the assemblage staurolite+cordierite+garnet+chlorite+andalusite+sillimanite+kyanite (biotite+muscovite+quartz+H₂O in excess) based on Fig. 2 of Dymoke and Sandiford (1992).

Figure 4 ($X_{Fe} = 0.7$) predicts a small range of existence for the staurolite-andalusite divariant assemblage, also that the divariant assemblage garnet-staurolite exists at much higher P and T than andalusite.

Figure 5 ($X_{Fe} = 0.8$), next page, predicts a greater range of P and T of existence for the divariant assemblage staurolite-andalusite. It also predicts that the assemblage containing garnet is displaced to lower P and T, due to an increase in Fe content.





X Fe = 0.8

Figure 5.

 Divariant field of staurolite-garnet

 Divariant field of andalusite-staurolite

Figure 5 predicts that increasing X_{Fe} will expand the andalusite-staurolite field to higher and lower T (525->600° C) as well as increasing the pressure range (3.4->4.2kb) that it is expected to occur over. Both the pseudo-sections for $X_{Fe}=0.7$ and $X_{Fe}=0.8$ predict that the assemblages garnet-staurolite and andalusite-staurolite do not occur together at similar pressures and temperatures.

Applications of this model system correlate well to the general assemblage variations (Dymoke and Sandiford, 1992) in the Southern Adelaide Fold Belt (see Fig 2). However, assemblages containing garnet-staurolite and andalusite-staurolite do occur together at close proximity's in the Southern Adelaide Fold Belt (Map 3, Appendix A). Indicating the need for reconsideration of the KFMASH system for these assemblage relationships

For mineral assemblage development equilibrium is assumed to have occurred in the system. This requires consideration of the minimization of Gibbs Free Energy, (G) where G is a function of (Pressure, Temperature and Composition). Mineral assemblages develop that attempt to minimize the local G.

Where small distances are considered pressure and temperature can be eliminated as variables of G minimization, so composition becomes the only variable. As stated the compositional system (KFMASH) is not sufficient to describe the existence of garnet with staurolite and andalusite, so other composition components not considered must be incorporated to describe the assemblage relations, and to minimize G for the composition present.

CHAPTER 3

Mineral Assemblages and Bulk Compositions of Meta-pelitic Rocks of Kanmantoo, South Australia.

3.1. Introduction

Chapter 2 introduced the importance of composition variation and the bearing that it may have on small scale (cm) mineral assemblage development. To develop this notion an outcrop 60 cm wide of meta-pelitic schist (Map 2, Appendix A) of Kanmantoo Group was divided into 18 separate samples (Map 3, Appendix A) perpendicular to the S_2 cleavage plane. This division was based upon small scale (cm) variations in the mineral abundances observed at the locality. The presence of garnet with staurolite signified this site as being representative of a change in bulk composition, which is transposed as a variation in mineral proportions. Distinction between the samples was made from assemblage variations noted in the field.

For each of these samples, bulk composition analyses were performed, as well as thin sections created for each of the samples. Table 1 presents the results for the bulk rock analyses in terms of weight percent (WT%), methods of analysis are outlined in Appendix D. All Fe_2O_3 was recalculated to FeO by use of a gravimetric standard of 0.89981.

The modal proportions of mineral assemblages were derived from point counting of thin-sections (Appendix B) and are shown in table 2. Mineral assemblages were defined for the samples by the existence of certain minerals within thin sections of the samples.

The discussion of the data received from analyses is conducted in three parts, as follows;

1. bulk composition variations in the samples are presented.
2. discussion of observed mineral assemblages.
3. comparison of mineral assemblages and MnO bulk composition variations.

	104a	104b	104c	104d	105i	105ii	105e	105w	106a	106b	107a	107b	107c	108	108 s	109	110	111
SiO2	61.91	57.07	61.59	62.2	66.42	64.17	62.91	62.66	56.69	61.67	61.61	49.95	62.14	58.05	58.19	58.5	59.19	58.71
Al2O3	17.96	17.17	17.2	18.92	16.44	16.97	13.23	18.35	14.85	15.98	13.11	12.33	12.67	16.73	19.64	16.79	18.92	19.37
FeO	6.89	7.46	8.46	7.72	7.35	8.18	11.21	8.95	16.08	10.24	14.37	20.80	14.20	11.29	11.63	11.14	10.02	9.86
MnO	0.07	0.08	0.1	0.08	0.12	0.11	0.18	0.11	0.5	0.09	0.4	0.26	0.41	0.09	0.1	0.09	0.12	0.11
MgO	3.43	3.45	3.7	3.12	2.72	2.89	4.61	3.05	3.24	3.54	2.73	2.39	3.32	3.69	3.58	3.61	3.47	3.64
CaO	1.05	0.66	0.42	0.42	0.21	0.24	0.24	0.25	0.52	0.21	0.38	0.22	0.36	0.27	0.21	0.27	0.25	0.21
Na2O	1.38	0.83	0.51	0.38	0.17	0.2	0.15	0.19	0.34	0.18	0.19	0.13	0.14	0.34	0.25	0.33	0.28	0.29
K2O	3.64	3.67	3.82	3.2	2.63	3.05	3.6	3.16	3.23	3.46	2.82	2.42	3.03	3.53	3.36	3.47	3.72	4.12
TiO2	0.76	0.77	0.77	0.84	0.71	0.77	0.63	0.84	0.63	0.75	0.46	0.45	0.49	0.76	0.79	0.76	0.76	0.79
P2O5	0.15	0.14	0.15	0.018	0.13	0.16	0.13	0.17	0.1	0.14	0.1	0.3	0.09	0.07	0.09	0.07	0.14	0.14
SO3	0	0	0	0	0	0	0	0	0.01	0	0.02	0.03	0.02	0	0	0	0	0
LOI	1.65	1.69	1.47	1.78	1.68	1.6	1.76	1.11	2.36	1.35	2.7	4.13	2.17	1.38	1.14	1.19	1.25	1.31
TOTAL%	98.89	92.99	98.19	98.68	98.58	98.34	98.65	98.84	98.55	97.61	98.89	93.41	99.04	96.20	98.98	96.22	98.12	98.55
X Al	0.633	0.610	0.584	0.634	0.617	0.603	0.453	0.602	0.428	0.535	0.428	0.345	0.414	0.526	0.562	0.531	0.582	0.587
X Fe	0.243	0.265	0.287	0.259	0.276	0.291	0.384	0.294	0.464	0.343	0.469	0.581	0.464	0.355	0.333	0.352	0.308	0.299
X Mn	0.002	0.003	0.003	0.003	0.005	0.004	0.006	0.004	0.014	0.003	0.013	0.007	0.013	0.003	0.003	0.003	0.004	0.003
X Mg	0.121	0.123	0.126	0.105	0.102	0.103	0.158	0.100	0.093	0.119	0.089	0.067	0.109	0.116	0.102	0.114	0.107	0.110
X Fe	0.663	0.679	0.690	0.707	0.721	0.732	0.701	0.739	0.811	0.738	0.821	0.887	0.792	0.749	0.760	0.751	0.736	0.725
X Mn	0.007	0.007	0.008	0.007	0.012	0.010	0.011	0.009	0.025	0.006	0.023	0.011	0.023	0.006	0.007	0.006	0.009	0.008
X Mg	0.330	0.314	0.302	0.286	0.267	0.259	0.288	0.252	0.163	0.255	0.156	0.102	0.185	0.245	0.234	0.243	0.255	0.267

Table 1 Bulk composition of sample space, from East - West

	garnet		staurolite		andalusite	muscovite prograde	retrograde	biotite	quartz
	small<0.5mm	large>0.5mm	relict	inclusioned					
104a	0	0	0	5	20	25	0	25	25
104b	1	0	0	5	20	25	0	25	25
104c	1	0	0	5	15	2	10	25	25
104d	0.5	0	0	10	20	40	5	15	10
105i	3	1	0	10	10	12	12	7	55
105ii	5	0	0	25	0	5	0	25	30
105e	1	5	0	35	5	0	2	25	25
106a	0	40	0	5	0	2	0	20	20
106b	2	3	0	40	0	15	0	20	30
107a	5	35	20	0	0	0	1	25	20
107b	0	15	35	0	0	0	0	20	20
107c	40	0	10	2	0	0	1	25	30
108	8	2	0	25	0	10	0	25	35
108s	12	3	0	40	0	0	0	25	30
109	5	10	0	35	0	0	5	15	25
110	5	5	0	35	5	20	5	25	25
111	1	1	0	25	20	15	0	20	20

TABLE 2. Modal proportions of minerals East (104a) to West (111) across sample space of 60cm.

3.2 Bulk Composition of sample space.

The bulk composition (Table 1) shows that there are significant variations in the components across the sample space, particularly in MnO, FeO and Al₂O₃. Low totals for the data are attributed to the water content and OH groups that are associated with the minerals. Two samples (104b and 107c) have totals too low for comparison, and are ignored, those totals above 95% are considered for comparisons to mineral proportions. The sample space reflects an East-West transition, where components MnO, FeO and SO₃ increase towards the middle, minerals Al₂O₃ and TiO₂, show a reverse trend by decreasing towards the middle of the sample space. Clarity on component variation across the sample space is given in the following section.

3.2.1. Variations in the sample space

Outlined is the calculated compositional variation (of key samples) from an outcrop of Kanmantoo schist. All further considerations are in reference to the proportions of Al, Fe, Mg and Mn (Appendix D), since mineral chemistry and probe analyses indicate that these are the major influential components in garnet development. Below are the calculated average proportions of the four elements for the entire sample space.

$$X_{Al} \text{ average} = 0.509$$

$$X_{Fe} \text{ average} = 0.330$$

$$X_{Mn} \text{ average} = 0.005$$

$$X_{Mg} \text{ average} = 0.103$$

The X_{Fe} ($X_{Fe} = \frac{Fe}{Fe + Mg + Mn}$) value of the samples lie in the range of 0.69-0.74, with a number of samples exhibiting values in the range of 0.8-0.82, see table 1, demonstrated in fig.6 below.

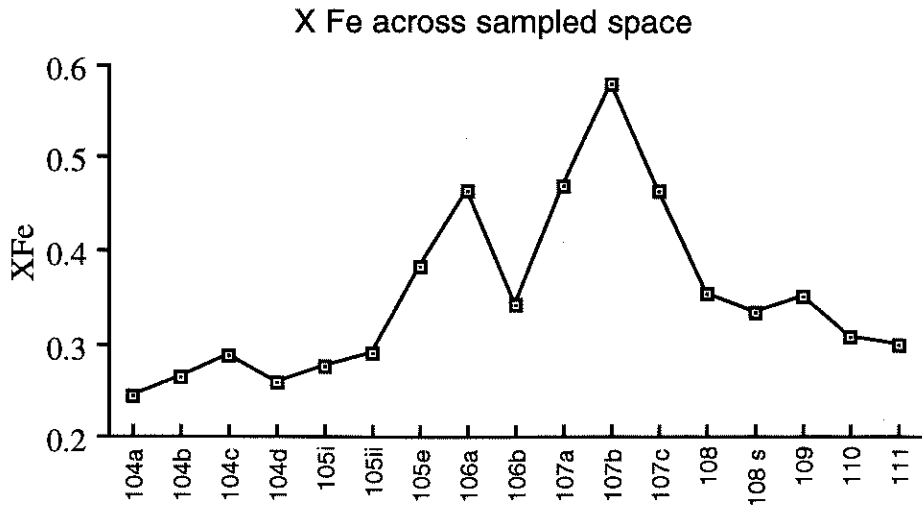


Fig.6 The X_{Fe} value for the sample space calculated from bulk composition.

The X_{Fe} range allows for the consideration of certain divariant mineral assemblages (of pseudo-sections of fig.4 and 5) to be applied these rocks, thus discussions on implications of assemblage formation can be performed. Other bulk components (MnO) can be shown to be influential, since the pseudo-sections do not predict the assemblage relations observed.

The variation across the sample space of the MnO component is shown by the calculation for X_{Mn} ($X_{Mn} = \frac{Mn}{Fe + Mg + Mn}$), represented by fig.7 below.

The majority of values, shown in fig. 7 lie in the range of 0.006-0.009, three samples however show much greater X_{Mn} values, (these are highlighted by fig. 10).

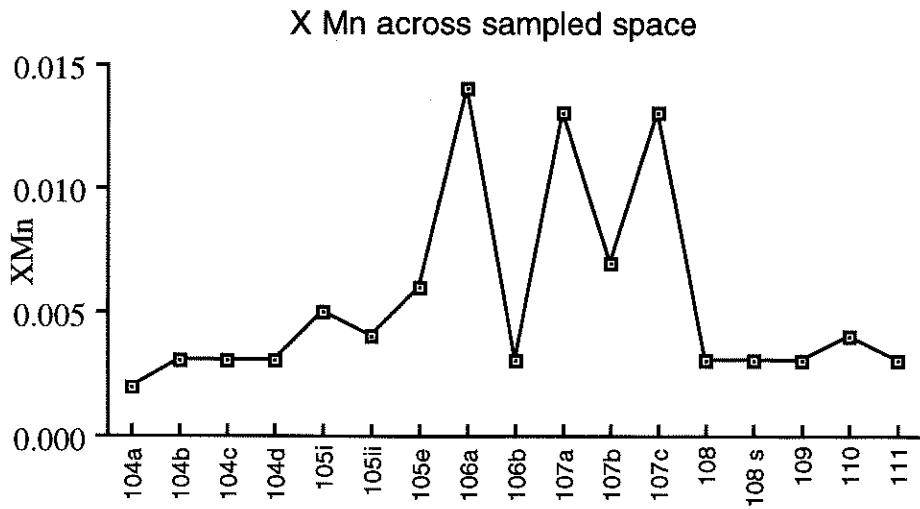


Fig.7 The X_{Mn} for the sample space calculated from bulk composition.

Figure 8 highlights the fact that Al₂O₃ content decreases for the “middle” samples, and that its content is much higher in samples deficient in the garnet phase (See table 2).

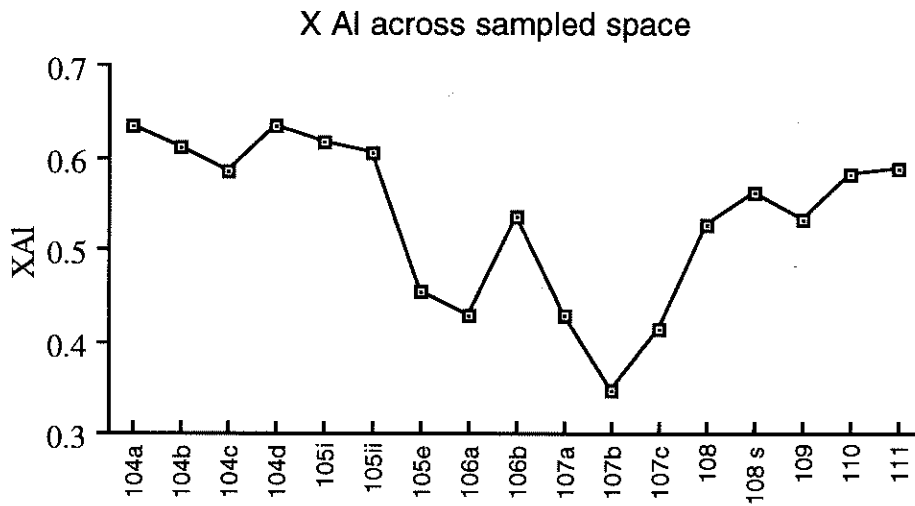


Fig.8 The X_{Al} for the sample space calculated from bulk composition.

Figure 9 reflects a similar trend as figure 8, where the MgO content decreases steadily from the “outside” samples until the greater garnet bearing samples are reached, where significant fluctuations are seen.

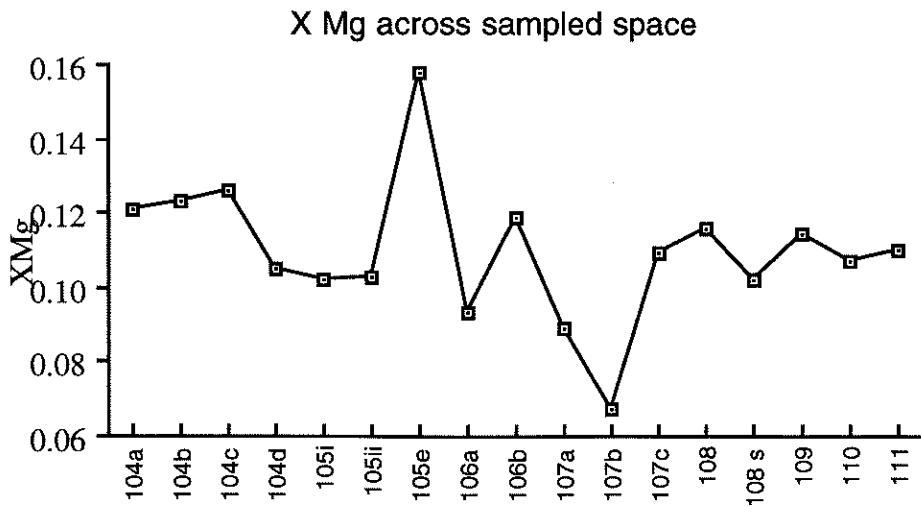
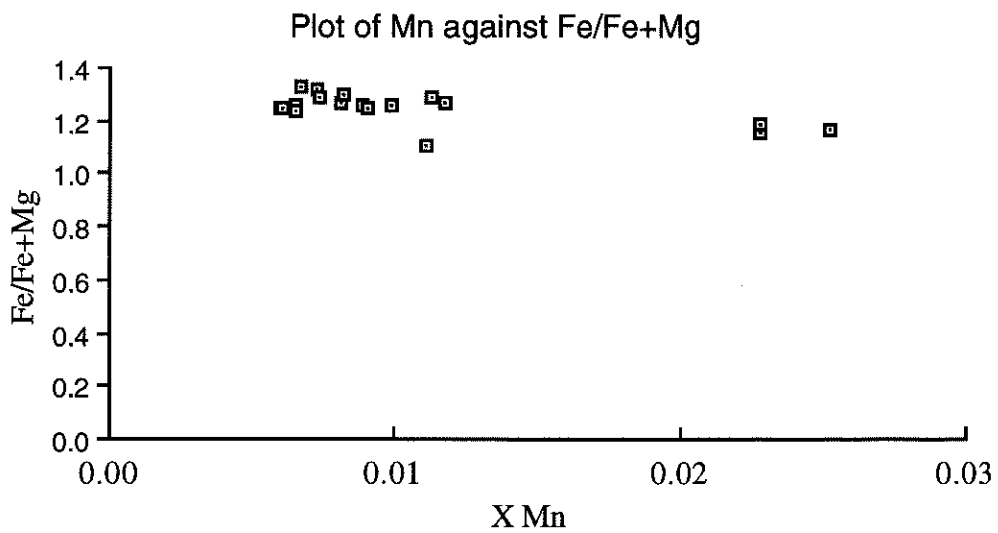


Fig. 9. The XMg value for the sample space calculated from bulk composition.

From a comparison of XMn versus $\frac{\text{Fe}}{\text{Fe} + \text{Mg}}$ (fig. 10 below) a constant $\frac{\text{Fe}}{\text{Fe} + \text{Mg}}$ ratio is seen for the sample space. However it can be seen that the three samples (106a, 107a and 107c) stand out distinctly from the rest of the sample space in terms of their Mn contents. The significance of these samples is discussed in light of the rest of the sample space in further sections.



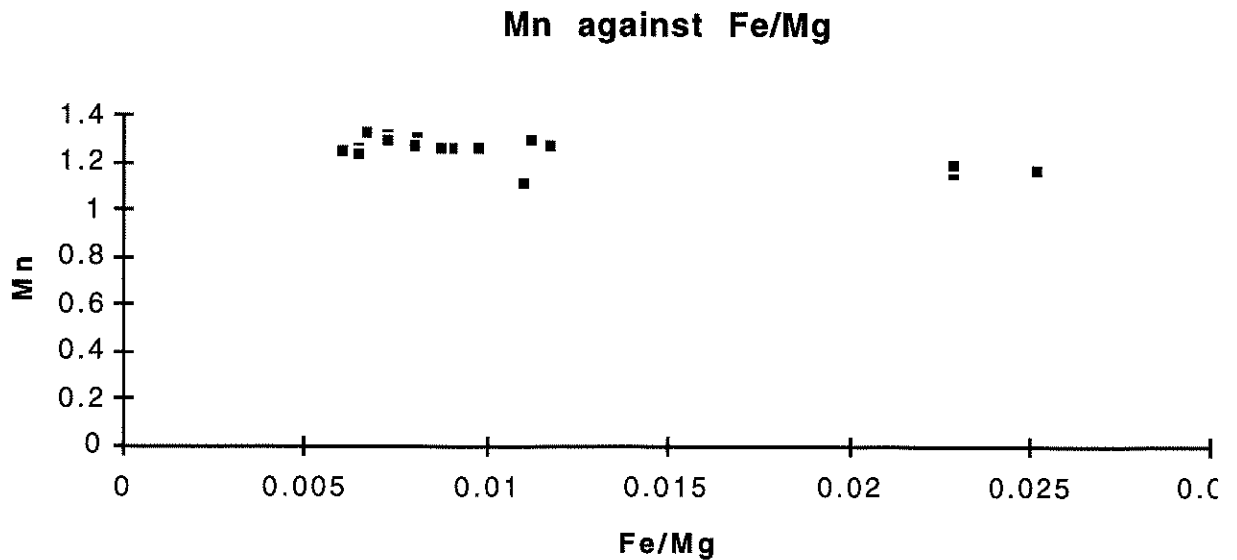


Fig. 10 Plot of X_{Mn} against Fe/Mg to highlight the variations in Mn in the sample space.

Summary

Predictions after Dymoke and Sandiford (1992) that additional components ie. MnO stabilise garnet at the expense of other minerals in Fe-rich bulk compositions are tested on real rock assemblages. The X_{Fe} values (Appendix D) of samples taken from schists are similar to those of the calculated P-T pseudo-sections and hence allow for the application of the model to real rocks. With this in mind further relationships between "minor" bulk compositional variation and mineral assemblage can be readily exposed.

3.2.2. Composition Variation within the Assemblages

Observations are discussed starting with the "simplest" assemblage, since this is the basis for all comparisons, other assemblages are presented in order of increasing garnet content. All discussion below is in referral to figs. 6, 7, 8 and 9, which represent the variation of the contents of the above mentioned components. The discussion highlights the samples which show the greatest compositional variation and provides a basis for the comparison in section 3.4.

The samples are discussed in an East to West fashion according to the assemblages that they contain. The minerals muscovite, biotite and quartz are not discussed since they are

considered to be in "excess" in the system and are involved in all mineral reactions. However, a few samples show interesting compositional relationships that require mention of the minerals muscovite and biotite.

Andalusite-staurolite assemblages

Sample 104a

From figs. 6, 7, 8 and 9 it can be seen that there is little deviation in the calculated component proportions from the "average" contents. Except that a higher than average X_{Al} is recorded, which is common with most of the samples. Lower than average X_{Fe} (0.243) and X_{Mn} (0.002) values are recorded, which appear to be typical for the extremities of the sampled area.

Andalusite-staurolite-garnet assemblages

Sample 104b will not be discussed since the bulk composition total (table 1) is below an "acceptable" level, even though it is the first sample (from the East) in which garnet appears.

Sample 104c

X_{Al} (0.584) is similar to those of 104a, however slight increases in both X_{Mn} (0.003) and X_{Fe} (0.287) relative to 104a are recorded. Importantly this is the X_{Mn} value of the first recorded occurrence of garnet in the system sampled.

Sample 105e

X_{Al} (0.453) drops below the average value for the first time from the eastern side of the sample space, similar to slide 109 (western side). However the X_{Mn} (0.006) value has increased above the average, similar to the X_{Fe} (0.384) which has also increased above the average to one of its maximums.

Sample 109

X_{Al} (0.531) drops to a value close to the average, whereas the X_{Fe} (0.352) for the first time on the western side of the sample space is greater than the average. X_{Mn} (0.003) has not varied from that of samples 111 and 104c.

Sample 111

X_{Al} is similar to many other calculated X_{Al} values, as it is greater than the average. Calculated X_{Mn} (0.003) is greater than that of sample 104a (0.002) and can be seen to correspond with X_{Mn} of sample 104c. The X_{Fe} (0.299) is much greater than sample 104a, but is still lower than the average value.

Staurolite-garnet assemblages

Sample 107b is not discussed here since the bulk compositional total is below an "acceptable" level.

Sample 106b

Aluminium content decreases at this locality with X_{Al} (0.535), to a value close to the average. Significant decreases are seen in the Fe and Mn contents where both X_{Mn} (0.003) and X_{Fe} (0.343) show a sharp reversal relative to the samples (106a and 107a) surrounding it .

Sample 108

The Al, Mn, Fe and Mg contents return to what could be called a "normal", relative to the sample space. The X_{Mn} value drops below the average, remaining consistent with the western side of the sample space, similarly X_{Fe} , X_{Al} and X_{Mg} values remain fairly consistent with other samples (108s-111) from the western side.

Sample 110

Component contents are consistent with the western side, except for X_{Fe} which drops below the average, similar to sample 111.

Sample 108s

Has similar compositional contents to that of sample 109, except for minor fluctuations (0.05) in X_{Fe} and X_{Al} .

Sample 106a

This sample records the one of the lowest X_{Al} (0.428), in a continuing trend of declination from sample 105e. The calculated $X_{Fe} = 0.464$ is one of the largest values recorded for the sample space so to is X_{Mn} (0.014) which reaches its peak for the sample space at this site. X_{Mg} shows an appreciable variation in value from those samples to its east.

Sample 107a

The aluminium content drops in this sample, to X_{Al} (0.428) with respect to the average, similarly the magnesium content drops as well. The manganese content shows an increase, with X_{Mn} peaking at 0.013.

Sample 107c

Is similar in compositional contents to sample 107a, except for a slight increase in X_{Mg} , from 0.89 (sample 107a) to 0.109.

Summary

From the data presented a number of comparisons can be made between different assemblages based upon their compositions. Comparisons are presented that show how proportions of components influence mineral abundance. These relationships are discussed in section 3.4.

3.3. Mineral Chemistry

3.3.1. Mineral Variations across sample space

Three mineral assemblages occur across the sampled space, they are listed below;

staurolite+garnet (+biotite+muscovite+quartz+feldspar+H₂O)

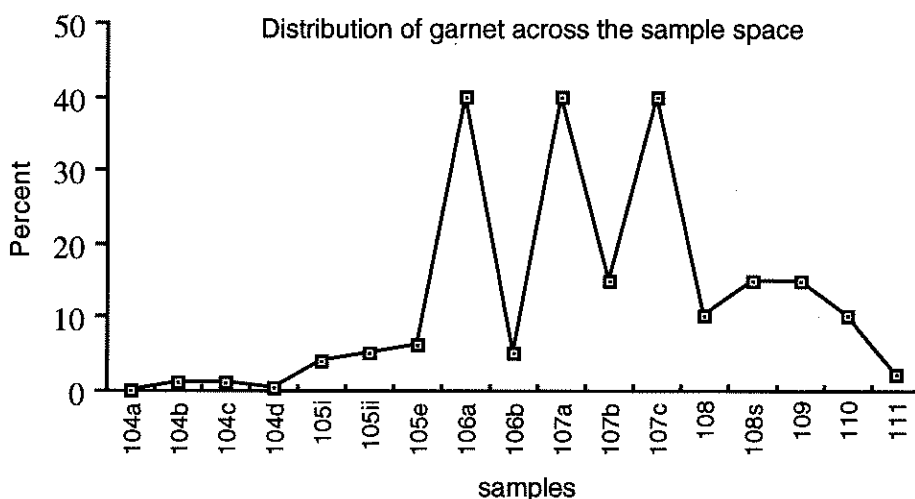
andalusite+staurolite (+biotite+muscovite+quartz+feldspar+H₂O)

andalusite+staurolite+garnet (+biotite+muscovite+quartz+feldspar+H₂O)

Detailed petrological descriptions of the sample texture and microstructure are given in Appendix B, since they are not necessary for the description of compositional variations within the phases. And so only simple mineral abundances are discussed in the following sections.

Plagioclase feldspars presence is ignored, since it does not participate in any relevant exchange reactions that need consideration, due to its non-existent Fe, Mn or Mg proportions.

The modal proportions of key metamorphic minerals (ie. garnet, staurolite and andalusite) contained in the above assemblages vary greatly across the sample space, see Table 2, graphs 1(a-c). It can be seen from table 2 and graph 1a, that the garnet phase is poorly represented in samples 104a-105e and 111, whereas samples 106a-110 have appreciable garnet content $\approx 15\text{-}40\%$. The modal proportion of the garnet phase can be seen to increase towards the centre of the sampled space (from the East and West), occupying nearly 40% of the rock in places.



Graph 1a. The distribution of garnet across the sample space in terms of percent occupation of the individual sample.

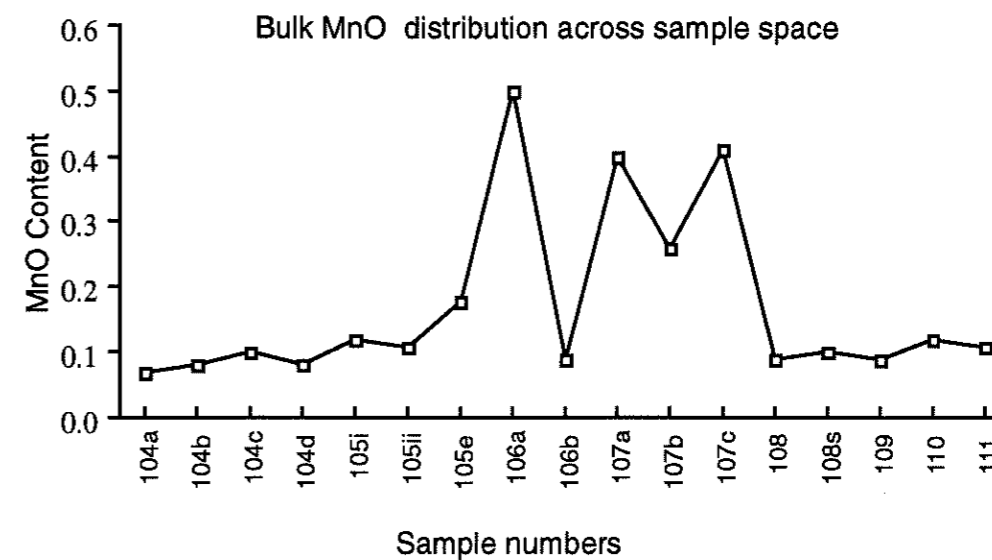
Contra to this, the modal proportions of andalusite (Graph 1b) can be observed to decrease from the "outside" samples (104a and 111) to the inner samples (106a-108s), where it is not represented at all.

Graphs 2-a and b.

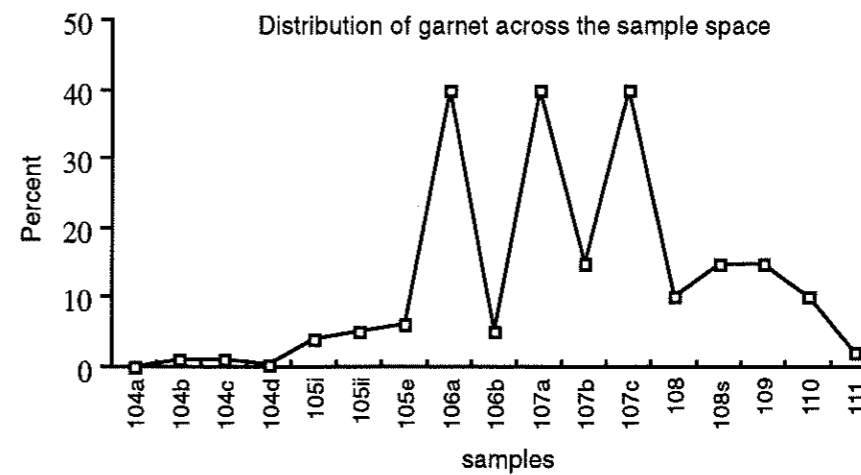
Graph 2-a. Bulk MnO composition variation across the sample space.

Graph 2-b. Variation in the modal abundance of the garnet phase across the sample space.

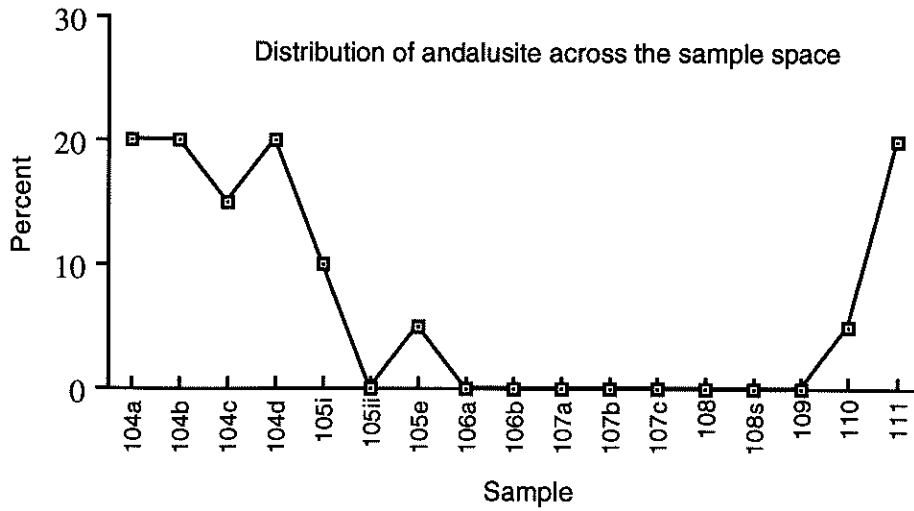
A comparison of these two graphs indicates a linear relationship between bulk MnO composition and garnet abundance *direct*



Graph 2-a. Distribution of bulk MnO across sample space.

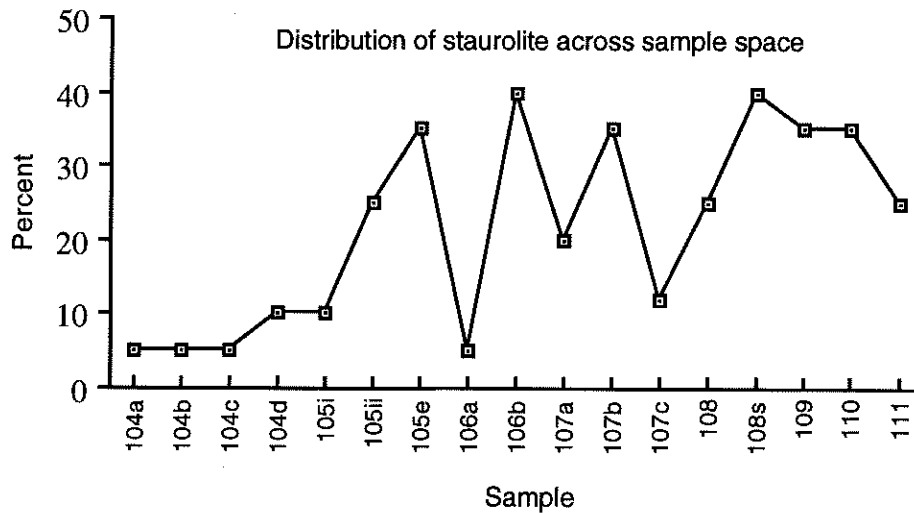


Graph 2-b Modal distribution of garnet across sample space.



Graph 1b. The graph of andalusite distribution across the sample space in terms of percent occupation of the individual sample.

The staurolite phase proportion also varies from east to west (Graph 1c) across the sample space, with generally lower proportions observed in the eastern samples (104a-d) to higher proportions in the western samples (110-111).



Graph 1c. The graph of staurolite distribution across the sample space in terms of the percent occupation of the individual sample.

3.3.2. MnO partitioning amongst minerals

The topic of interest is the role that MnO has on the development of garnet in mineral assemblage, so the distribution of the components amongst the minerals is an important point that must be highlighted before any further discussion of bulk composition.

Mineral formulas listed in table 3 below outline the distribution of components amongst the phases of consideration.

Support for this is provided by micro-probe analysis (performed on minerals of selected samples, Appendix C), where it can be seen that the MnO component is preferentially partitioned into the garnet phase occupying $\approx 1-7$ WT%. Probed staurolites show that MnO accounts for less than 0.643 weight percent (WT%), most values are recorded in the range of 0.04 -0.2 (WT%). Biotite analysis show that MnO accounts for less than 0.25 (WT%) with most values in the range 0 -0.15 (WT%). Muscovite shows a similar trend, with MnO values in the range 0 -0.191 (WT%), with the greater number in the range 0- 0.1 (WT%).

Because of this partitioning, all MnO in the system is considered to be incorporated into the garnet phase only and all further treatments of MnO are in accord with this assumption.

Andalusite	Al_2SiO_5
Staurolite	$(\text{Fe}^{2+}, \text{Mg})_4 \text{Al}_{18}$ $\text{Si}_{7.5} \text{O}_{48} \text{H}_4$
Garnet	$(\text{Mg}, \text{Fe}^{2+}, \text{Mn})_3 \text{Al}_2 \text{Si}_3 \text{O}_8$
Muscovite	$\text{K}_2 \text{Al}_4 [\text{Si}_6 \text{Al}_2 \text{O}_{20} (\text{OH}, \text{F})_4]$
Biotite	$\text{K}_2 (\text{Mg}, \text{Fe}^{2+})_{6-4} (\text{Fe}^{3+}, \text{Al}, \text{Ti})_{0-2}$ $[\text{Si}_{5-6}, \text{Al}_{3-2}, \text{O}_{20}] (\text{OH}, \text{F})_4$
Plagioclase Feldspar	$\text{Na} [\text{AlSi}_3 \text{O}_8] - \text{Ca} [\text{Al}_2 \text{Si}_2 \text{O}_8]$

Table 3 Mineral formulas of muscovite, biotite and plagioclase feldspar are after Deer, Howie and Zussman, 1992, those of garnet, staurolite and andalusite are after Holland and Powell, 1990.

When comparing bulk composition to the observed mineral assemblages, (graph 2a-b) it can be seen that MnO WT% corresponds closely to the garnet assemblage representation. This initial observation is examined in greater detail. Selected samples are examined to establish a correlation between variations in MnO content and garnet presence and proportions.

3.4. Comparison of mineral assemblages and bulk composition

As the composition profiles (discussed in the next chapter) are a result of growth processes, comments can be made in light of the effect that various components may have had on influencing mineral growth, ie. MnO on garnet crystallisation. To do this, a comparison is made between assemblages containing garnet and those devoid of garnet. So a "normal assemblage" is defined, ie. a garnet "free" and MnO "absent" assemblage is used as a basis for comparison of all other garnet "bearing" assemblages.

A comparison is made between bulk composition and mineral assemblage. More precisely the relationship between garnet and bulk MnO composition can be highlighted. This is performed via ternary diagrams constructed for the system A, F and Mn, by projecting from biotite, muscovite, quartz and H₂O (KMSH).

3.4.1 Discussion of Data

Predictions from a T- X_{Fe} pseudo-section calculated by Dymoke and Sandiford (1992), (fig. 11) form a basis for a comparison of mineral assemblages sampled. Garnet bearing mineral assemblages are predicted to occur above $X_{Fe} > 0.8$ (due to the strong partitioning of Fe²⁺ into the garnet crystal). This is not the situation for this sampled section, as outlined previously as garnet assemblages are found below $X_{Fe} > 0.8$. By considering the component MnO a better description of the mineral assemblage relationship at this locality can be performed.

FIGURE 11.

Calculated isobaric T- X_{Fe} pseudo-sections calculated from Fig.2 of Dymoke and Sandiford (1992), at a pressure of 4kbar. Importantly the garnet+staurolite divariant assemblage occurs at higher X_{Fe} than the divariant assemblage andalusite-staurolite. This permits the introduction of another component, which explains the displacement of the divariant garnet-staurolite to lower X_{Fe} .

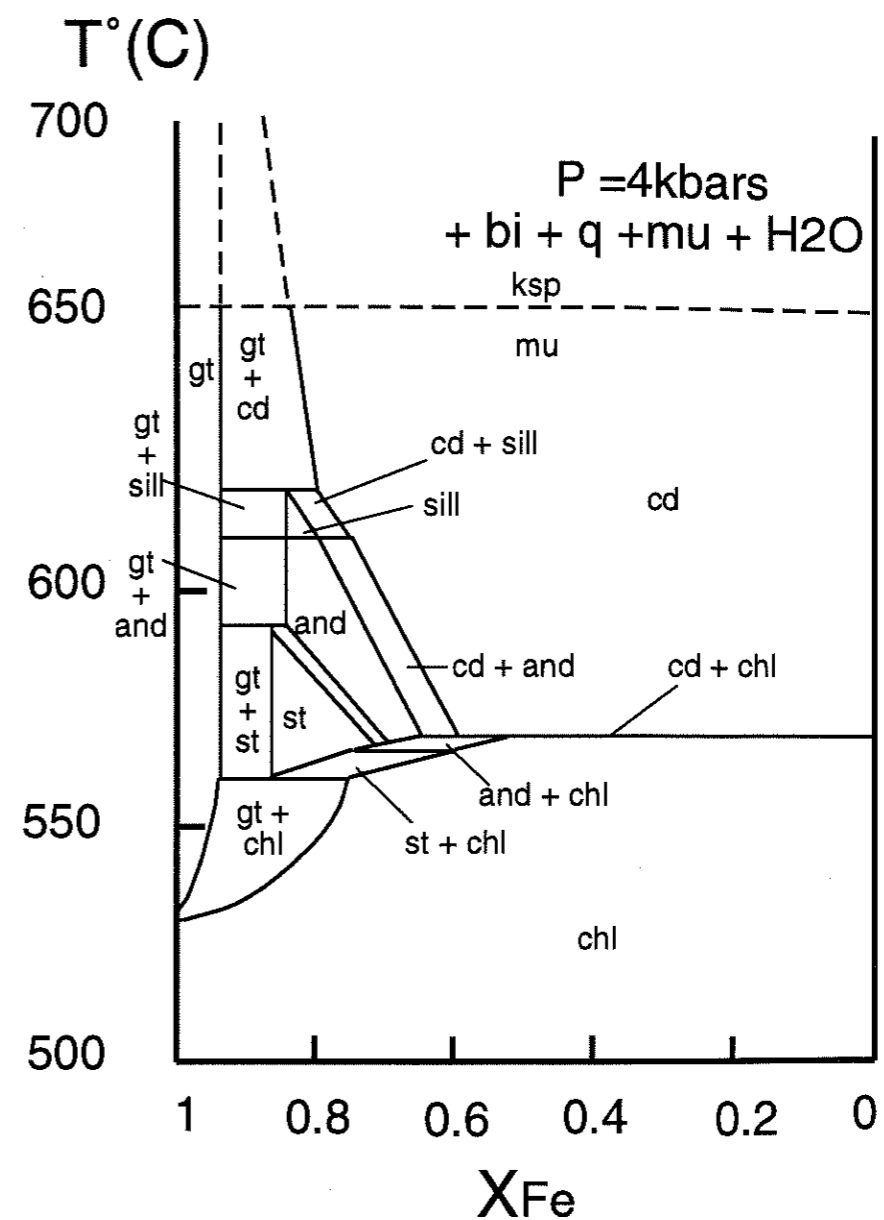


Figure 12.

Selected samples are represented in AFM diagrams (+muscovite+quartz+H₂O in excess). These were created from data contained in Appendix C.

Diagram a is the “normal” AFM since it contains no garnet and it forms a reference for comparison of all other samples.

The diagrams (b-e), highlight the need for an expanded component system to describe the assemblage relations observed, since crossing tie-lines exist between staurolite-biotite and garnet-biotite.

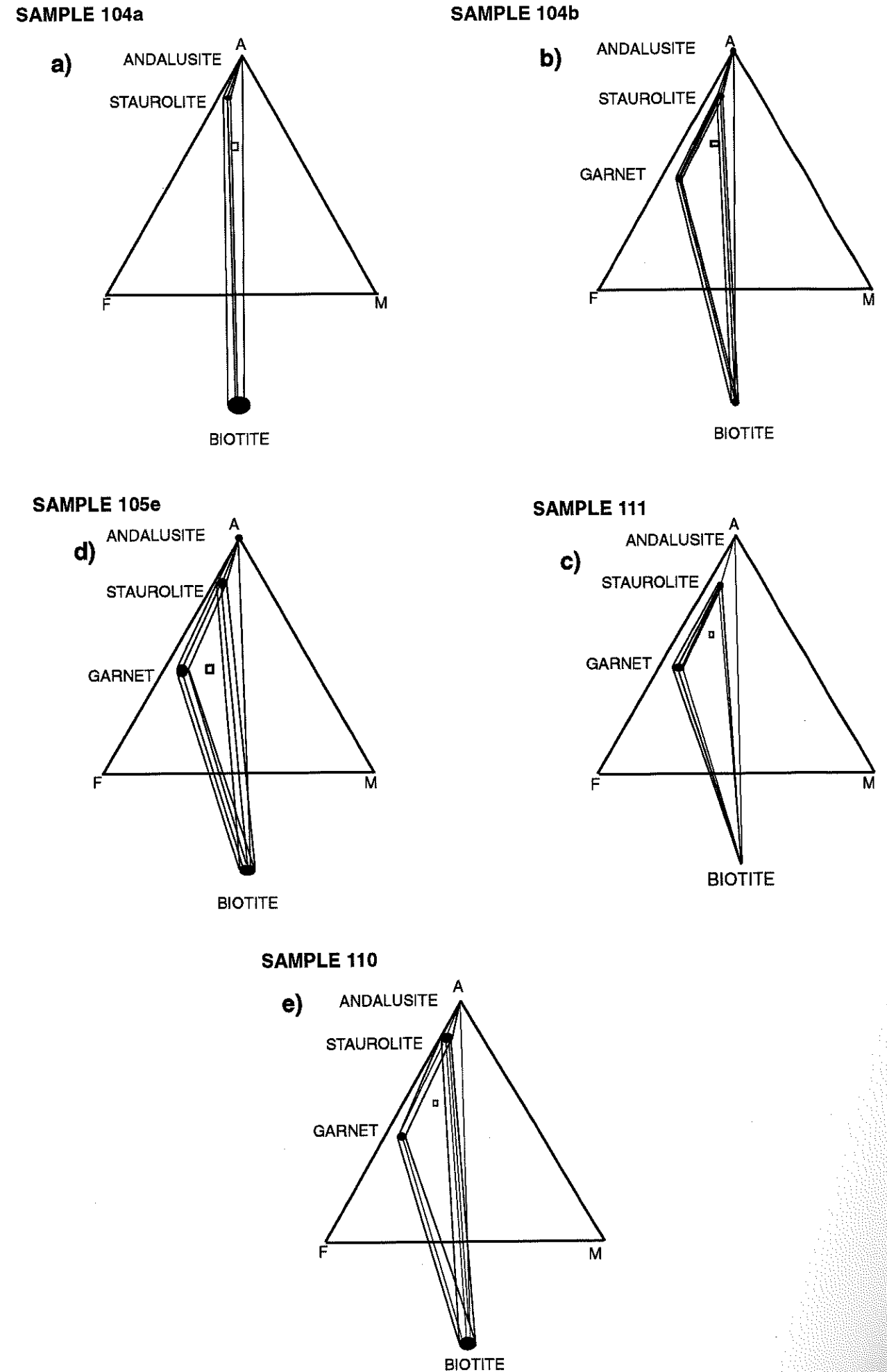


Figure 12 a-e

Figure 13.

AFMn diagrams (+biotite+muscovite+quartz+H₂O) are presented for samples created from data contained in Appendix C. They demonstrate that small amounts of MnO influence the development of garnet with assemblages (andalusite and staurolite) that the KFMASH system (AFM) can not account for. The diagrams show that apparent crossing tie-lines in AFM are not what they appear. The addition of the Mn component perpendicular to AFM shows that the tie-lines do not cross, and that small amounts of Mn are sufficient to permit the formation of garnet with andalusite-staurolite assemblages.

The diagrams b-j (next page), show that bulk composition (square box) reflects the assemblage proportions for the individual samples, which is a consequence of the bulk MnO content.

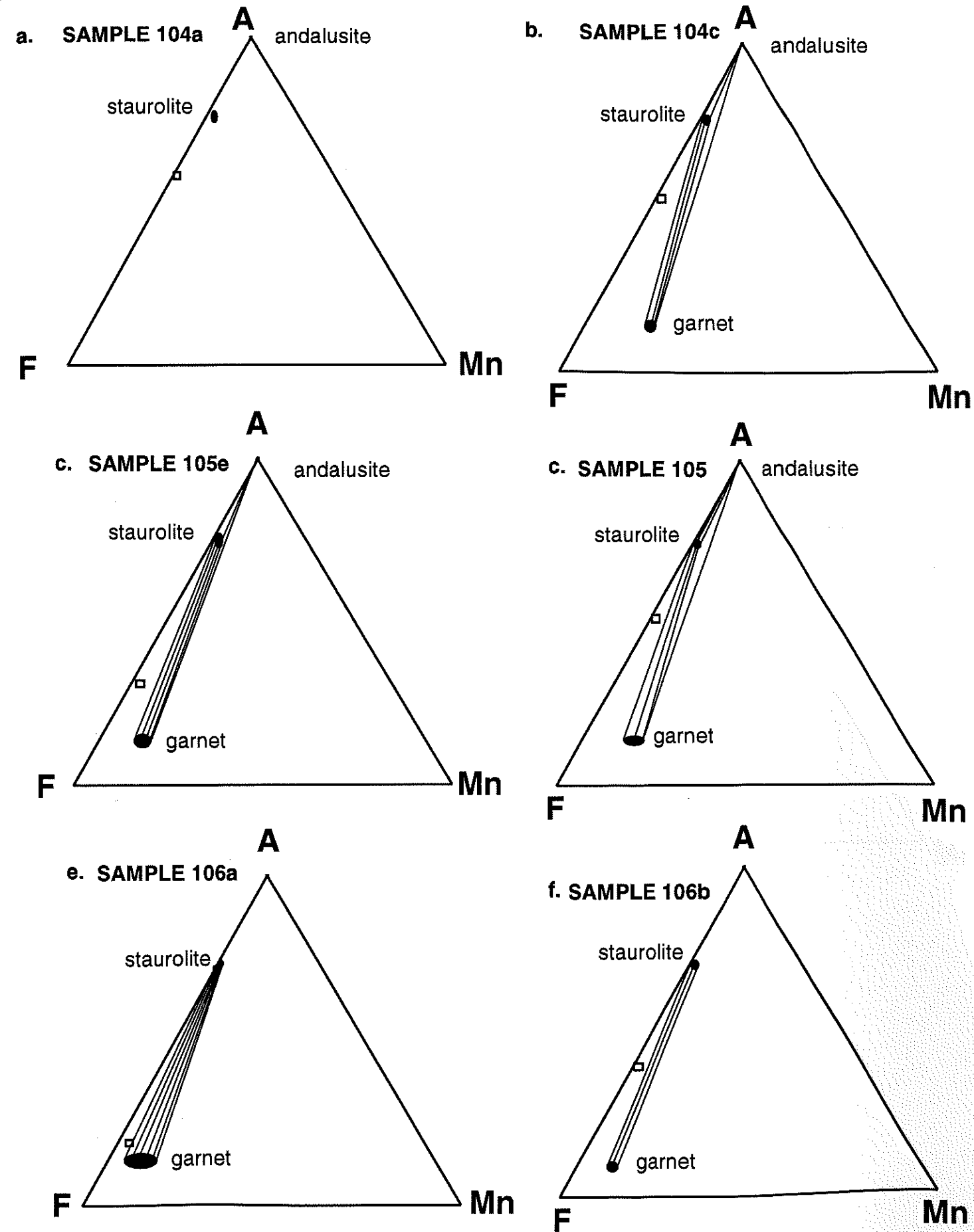


Figure 13 a-f. AFMn diagrams for samples, constructed from AFM diagrams all assemblages projected from bi + mu + qtz + H₂O

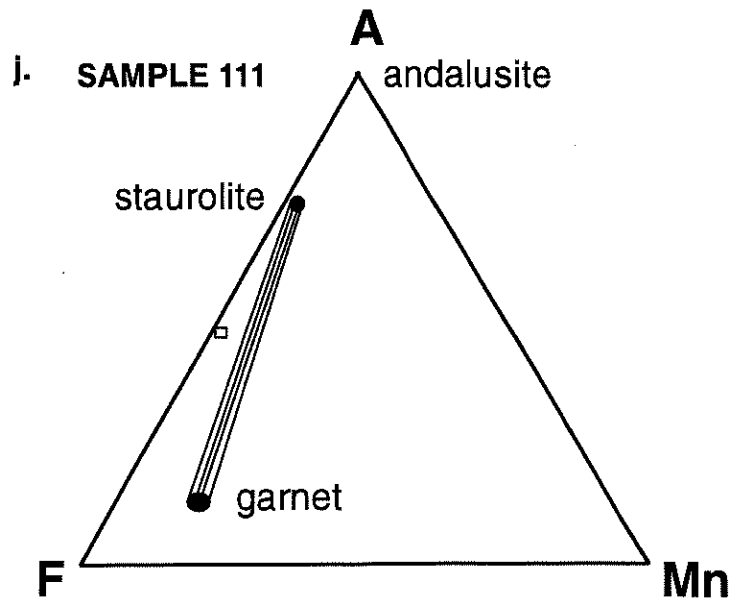
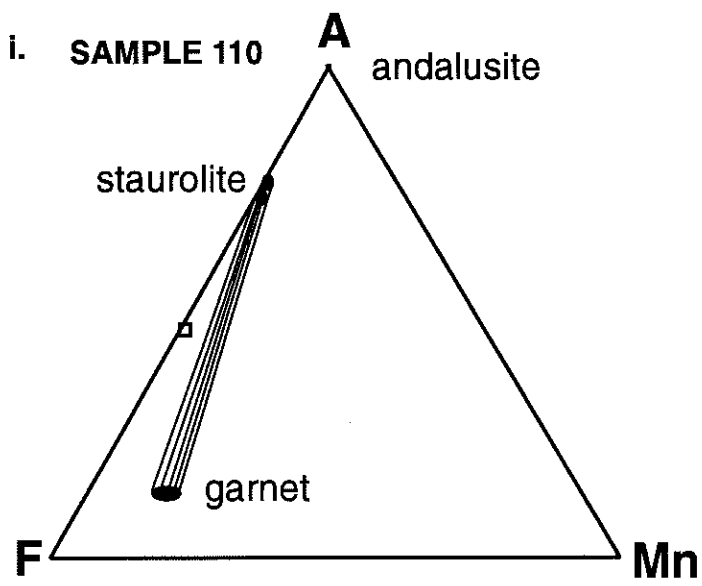
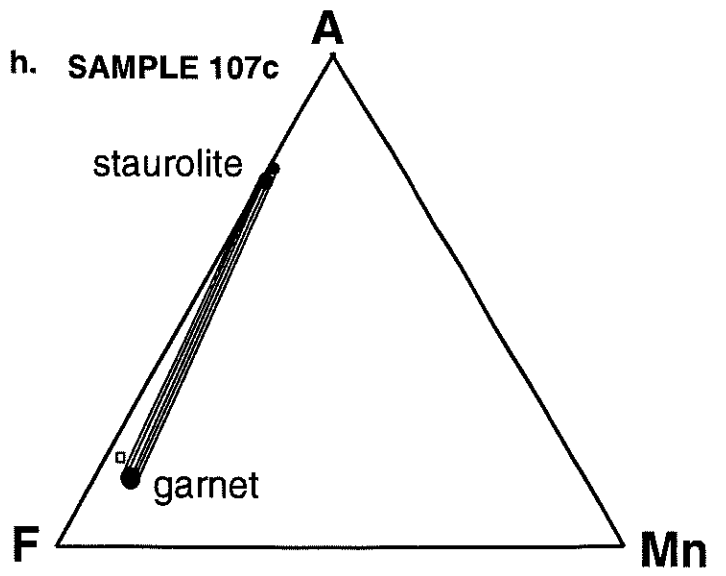
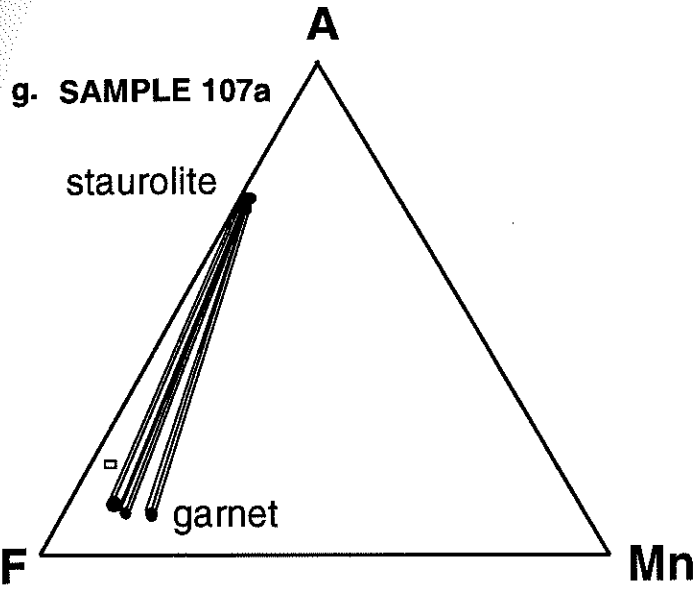


Figure 13 g-j. AFMn diagrams for samples, constructed from AFM diagrams of all assemblages projected from bi + mu + qtz + H₂O

The following section presents the relationships between the mineral proportions, bulk compositions and mineral compositions (represented as ternary diagrams) for the minerals in the separate samples. The "normal assemblage" ie. andalusite-staurolite, is used as a basis for comparison for other assemblages that differ to it. Comparisons are made between different samples to show the relative assemblage dependence on bulk composition. Phase diagrams constructed (from data in Appendix C) for the system AFM (+muscovite+quartz+H₂O) are shown in fig.12. These form a basis for the projection through biotite onto the AF plane allowing for the addition of Mn (fig. 13) to the system (+biotite+muscovite+quartz+H₂O) for description of the garnet phase.

Andalusite-staurolite assemblages

This assemblage is considered to be the most simple represented in the sample space. The bulk composition is considered as a basis for comparison of other assemblages for the sample space.

Sample 104a

Ternary diagram construction in the system AFM (fig.12-a) reveals a simple 3-phase mineral assemblage(+muscovite+quartz+H₂O), further projection into AFMn (fig.13-a) space was performed for comparison of other assemblages. The lack of garnet agrees with the predictions of fig.11 for X_{Fe} values of this magnitude. This is reflected by the simple tie-line relationship in fig. 12a.

Andalusite-staurolite-garnet assemblages

Primary variations in the proportions of minerals present in other samples is shown by comparison to sample 104a. A new phase (garnet) has developed in the system, which provides complications for projecting the new mineral assemblage in AFM. Crossing tie-lines become apparent between staurolite-garnet and staurolite-biotite phases (fig. 12a-e), these conjectures in the AFM projection can be "explained" by the incorporation of another component (ie.MnO) to the system. By projecting the minerals through biotite onto the AF plane a new component Mn can be used to describe mineral relationships more clearly. Predictions by fig.11 for rocks with X_{Fe} of this range can not describe the mineral assemblage observed at this X_{Fe} (in

KFMASH), however, with the introduction of small amounts of MnO to the system, these divariant fields are displaced to lower X_{Fe} values.

Selected samples represented by AFM diagrams presented in Figure 12b-e highlight the necessity for the introduction of another component to describe the mineral assemblage present. The introduction of another component (Mn) perpendicular to the AFM plane describes the mineral relationships without the occurrence of crossing tie-lines.

A sufficient Mn content in sample 104c (fig.13-b) is able to describe the crossed tie-lines in fig.12b, where the garnet is observed to reside "above" the AFM plane. Similarly sample 105e (fig.13-c) shows this relationship as well, as do samples 105, 110 and 111 (figs. 13-d,13-k and 13-l respectively). The formation of the garnet phase can be seen to be a function of an incremental increase in bulk MnO content. This notion is supported by changes in garnet proportion as a response to variations in bulk MnO content, shown by comparisons between assemblages devoid of the andalusite phase.

Staurolite-garnet assemblages

The prediction that garnet crystalization is assisted by the presence of small amounts of MnO is shown above. This relationship is further developed and supported by the variations in modal abundance of garnet with bulk MnO content, seen in samples of this assemblage. This is best observed in a comparison between samples 106a and 106b, where significant variations in MnO content (fig. 13-e and f) are reflected in the modal abundance of the garnet mineral (graph 2-b). In sample 106a (fig.13-e) it can be seen that the bulk composition approaches the garnet phase in accordance with an increased modal proportion of garnet. This relationship is reversed in sample 106b (fig.13-f) where the "low" MnO content is reflected in the poor representation of the garnet phase, thus the bulk composition plots further away from the garnet phase in AFMn.

Similarly these assemblage relationships are supported by the sample series 107 a-c, where variations in bulk MnO are proportional to the modal abundance of the garnet mineral (graph 1). The bulk compositions of these samples reflect this

relationship, where in samples 107a and 107c (Fig. 13-g and h) it can be seen to approach the garnet phase in AFMn.

3.4.2. conclusions

An inverse relationship is presented (graph 3) between the MnO WT% of garnets and the bulk compositions of the samples. This inverse relationship is attributable to the size of the garnet population, and hence the bulk MnO composition at the onset of crystallisation. It is proposed that sites of crystallisation were fewer in these assemblages, so the MnO was partitioned between less individual garnets, so more MnO was incorporated into the garnet phase than samples with greater garnet proportions. This is reflected in MnO profiles for garnets, which are higher in the core and decrease towards the rim, this trend implies a change in the availability of the MnO during garnet growth. The bulk compositional availability of MnO, controlled garnet growth. Garnet growth ceased once the MnO available within a certain radius of the surrounding matrix became depleted, this radius was defined by matrix diffusional processes.

CHAPTER 4

Distribution of MnO in garnet across the sample space.

Consideration must be made of how the components are distributed amongst the minerals of the assemblages in the samples.

It has been shown in both theory (Howell, 1991) and in real systems (Symmes and Ferry, 1992) that the fields of mineral assemblages of KFMASH are displaced by the addition of small amounts of MnO. Variation in the distribution of MnO, FeO, MgO and Al₂O₃ in the minerals is shown by selected probe analyses (Appendix C). Late stage diffusion processes are ignored so all profiles can be considered to be due to growth.

What is presented below is the trend from selected MnO profiles across garnets from samples of the different assemblages. This shows the distribution of MnO amongst the garnet populations of variable bulk MnO compositions.

The Mineral Assemblages

4.1. Andalusite-staurolite assemblages

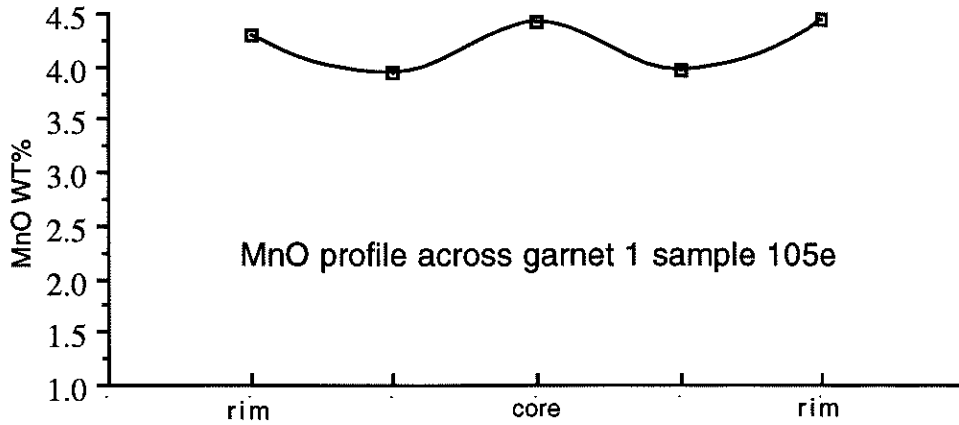
No garnets were observed in the sample to be analysed.

4.2. Andalusite-staurolite-garnet assemblages

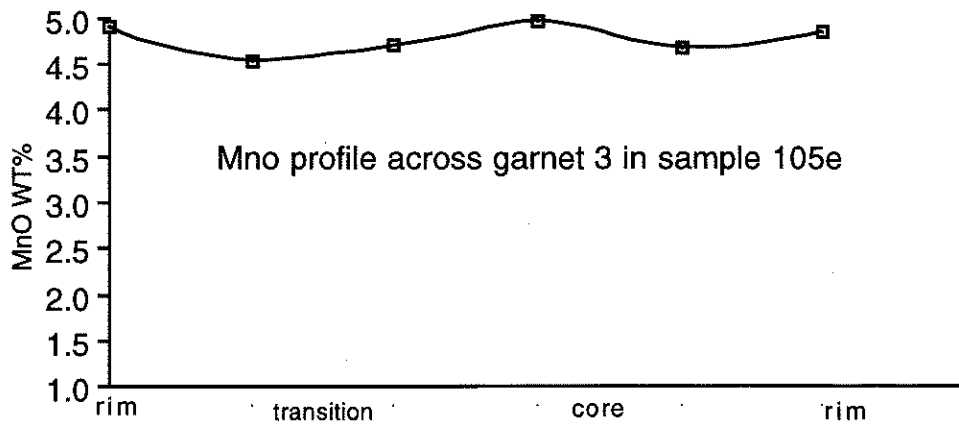
Samples of this assemblage demonstrate the important feature that a relationship exists between the distribution of MnO in garnets and the bulk MnO composition of the garnet bearing assemblage.

Sample 105e

The MnO content of garnet (graphs 4a and 4b) is slightly lower (≈ 4.5 WT%) when compared to garnets of sample 111 (graph 4c). Implying that MnO is dispersed further amongst the garnet crystals, this is due to the higher bulk MnO content which allows for greater garnet development, hence MnO is partitioned further between the developing garnet crystals.



Graph 4a MnO profile across garnet #1, data listed in Appendix D.

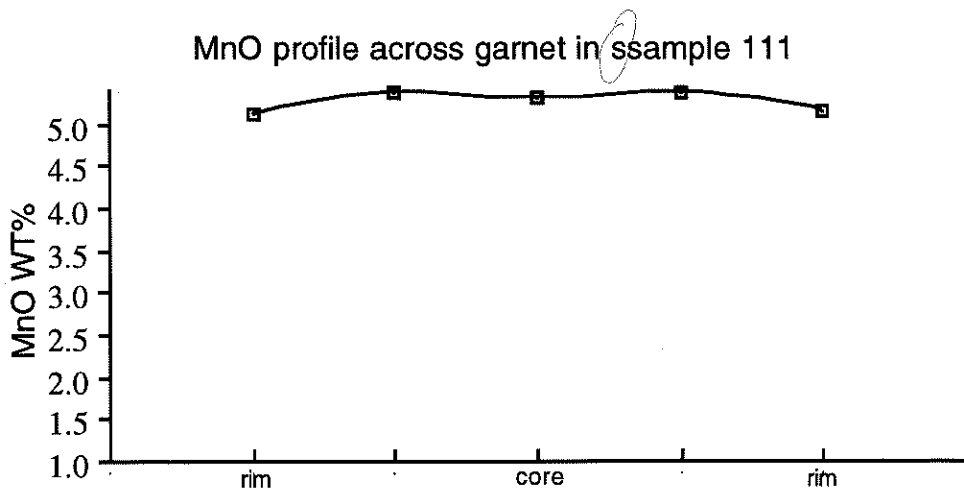


Graph 4b MnO profile across garnet #2, data listed in Appendix D.

Sample 111

These analyses reveal that MnO typically occupies a greater WT% (≈ 5.30) of the garnets here than in samples of other assemblages ie. 106a and 108s (≈ 3.5 and 4.0 WT% respectively), which have greater modal proportions of garnet. This is due to its Bulk MnO content, which is sufficient for garnet development. The content permitted garnet development up until a point in time where Mn was consumed, after which the Fe and Mg was incorporated into the developing staurolite phase. This

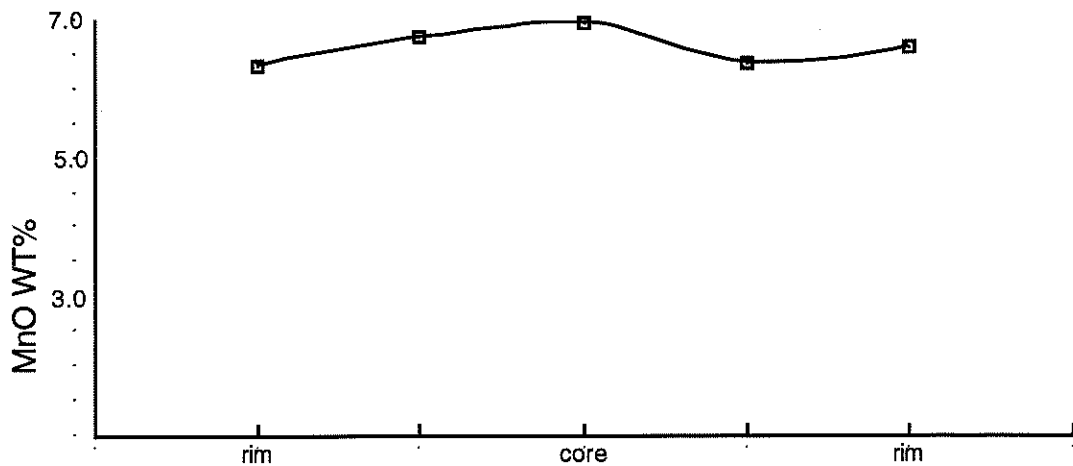
reflected in the textures, where staurolite is seen to envelope garnet crystals (Appendix B).



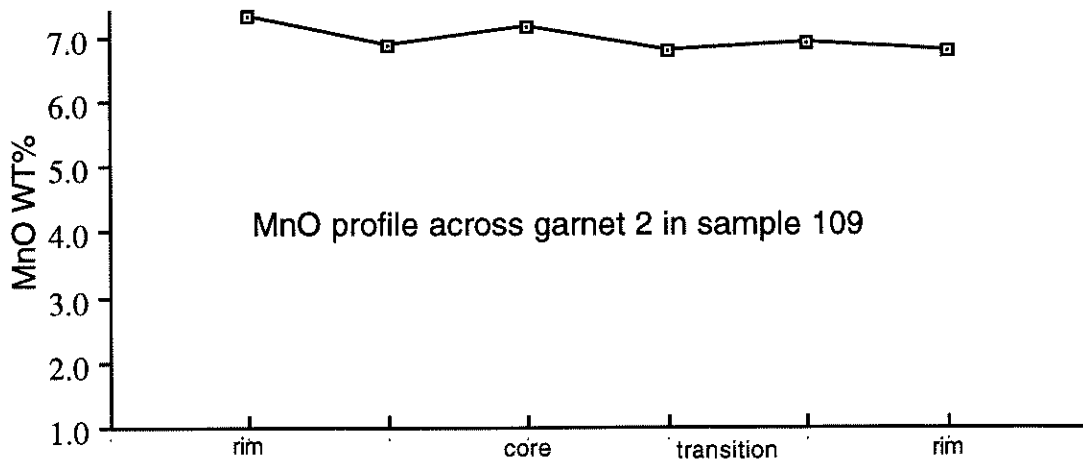
Graph 4c MnO profile across garnet from sample 111, data listed in Appendix D

Sample 109

Probe results for garnets have higher MnO contents (6.7-7 WT%) (Graphs 4d-4e) than those of sample 105e, which is in accord with relationships described before in sample 111. This "lack" of variation is typical for the samples with low bulk MnO content.



Graph 4d. Profile across garnet #1, data contained in Appendix C.



Graph 4e. Profile across garnet #2, data contained in Appendix C.

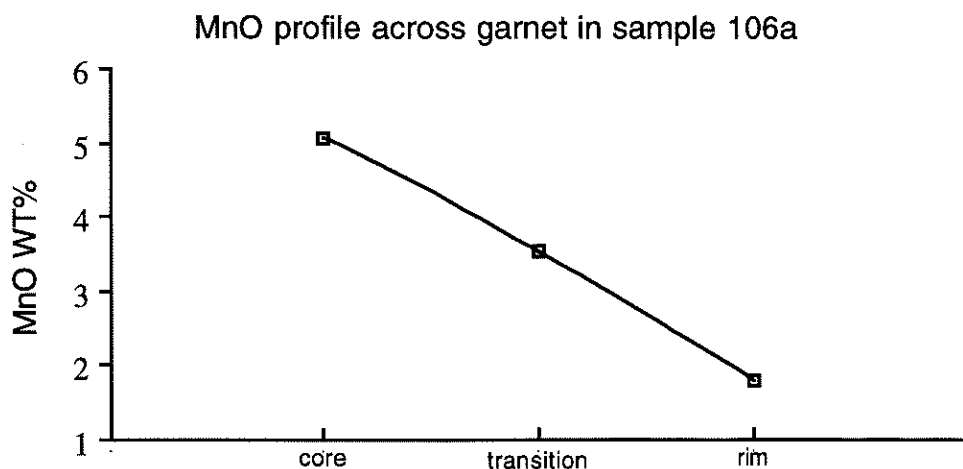
SUMMARY

The inverse relationship presented (graph 3) between the MnO WT% of garnets and the bulk compositions of the samples is highlighted by samples of this assemblage. This inverse relationship is attributable to the bulk MnO composition at the onset of crystallisation. MnO content was sufficient to initiate garnet development, so Mn was partitioned quickly into the garnet, though low bulk Mn content controlled garnet development, so garnet growth was not prolific. Garnet growth ceased once the MnO available within a certain radius of the surrounding matrix became depleted, this radius was defined by matrix diffusional processes. Once garnet development stopped Fe became available for other minerals to develop (which staurolite was the next, see Appendix B). This is reflected in the textures described in Appendix B.

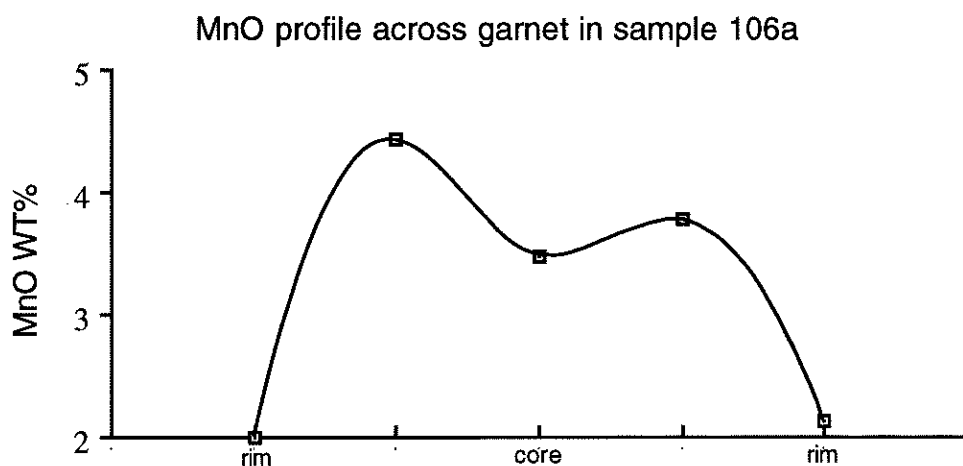
4.3. Staurolite-garnet assemblages

Sample 106a

Of importance is the magnitude of MnO WT% depletion from the core to the rim in garnets (as seen in previous samples), which appears to be common to the samples with higher MnO compositions, graphs 4f and 4g.



Graph 4f. MnO profile across garnet #2, data from Appendix D.



Graph 4g. MnO profile across garnet #1, data from Appendix D.

Garnet profiles (graphs 4 f-g) show a depletion in MnO towards their rims, which indicates that the availability of MnO was depleted towards the end of its growth. Muscovite present in the matrix is distanced from garnet in the matrix, suggesting that MnO availability controlled growth rates and not the muscovite (predicted from the reaction below).

staurolite + muscovite

= garnet + aluminosilicate + biotite (+ quartz, H₂O).

The MnO content in garnets varied throughout the sample (as shown by graph 3) indicating that some garnets incorporated more MnO in the early stages of their development than others. A decrease in MnO content occurs towards the rim of the garnet, similar to garnets in samples 111, 108s and 109 (graphs 4c, 4d, 4e and 4l), implying Mn exhaustion caused the cessation in garnet growth, (Table 2).

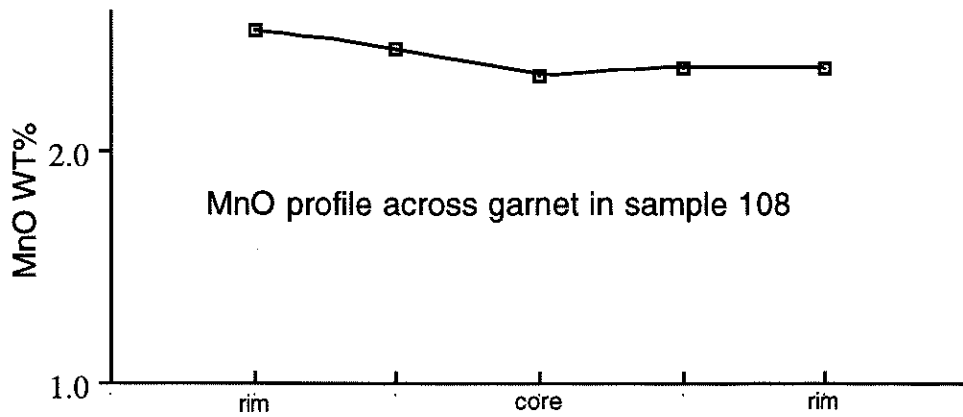
The density of the garnet population is high as the modal proportion indicates, hence the overall MnO contents in the garnets is lower than those samples with considerably smaller garnet populations.

Sample 106b

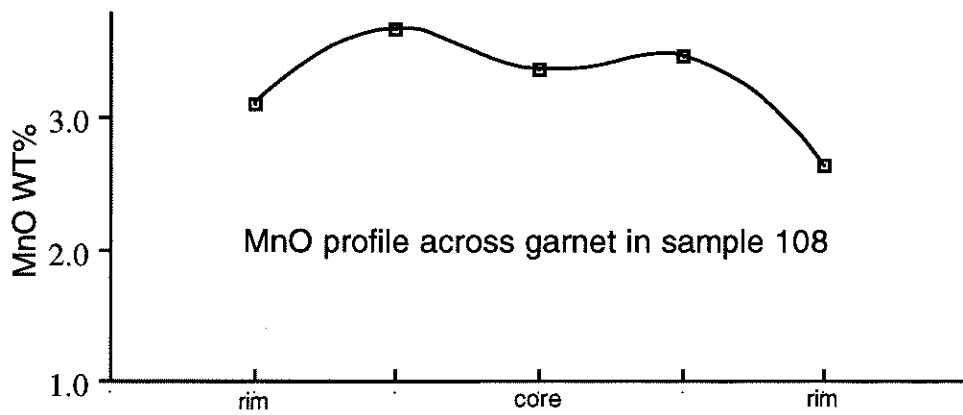
The only garnet core probed gave a low MnO WT% (3.766 WT%), which corresponds with the results from sample 106a. It is not inconceivable that the garnets in both samples are in fact part of the one "population" that was divided during sampling. But the fact remains, that the bulk MnO composition of the rock (defined by the sampling boundary) is reflected in the garnet growth.

Sample 108

Importantly these profiles (4i and 4j) reflect an decrease in magnitude of MnO variation across garnets within the sample space, whilst still maintaining relatively small overall MnO WT%.



Graph 4i MnO profile across garnet from sample 108, data contained in Appendix D



Graph 4i MnO profile across garnet from sample 108, data contained in Appendix D

Sample 110

The MnO WT% profile (rim-core-rim) from a small matrix garnet (not shown) is higher ie. 6.175-5.198-5.443, than those of the "central" samples. The variation in the garnet profile, relative to the garnet of sample 106a is small, and is constant with the low variations in the profiles of the "low" MnO samples.

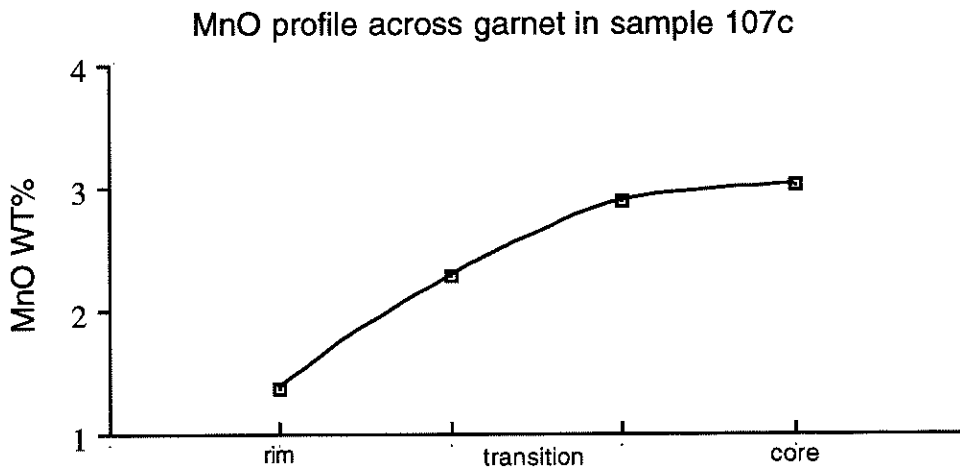
Sample 107b

The lack of data does not serve to highlight the relationship of MnO and garnet at this site. The important relationship observed here is a different morphology of staurolite from the rest of the sample space, described as "relict". The MnO content here is lower than sample 107c (0.23 WT%), and the garnet phase is far less represented in the sample space ($\approx 15\%$) when compared to sample 107c ($\approx 40\%$ garnet). Garnet growth continued until Mn was exhausted, the high Fe allowed for the development of a later phase of staurolite which grew and deformed the rest of the fabric, see Appendix B.

Sample 107c

These analyses are consistent with previous results, in that the magnitude of MnO variation across the garnet profile is greater than "low bulk" MnO garnet profiles.

Profiles in garnet (Graph 4k) show greater differences from the rim to core (1-2 WT%), a magnitude that was not seen in profiles of other samples ie. 109,110 and 105e.

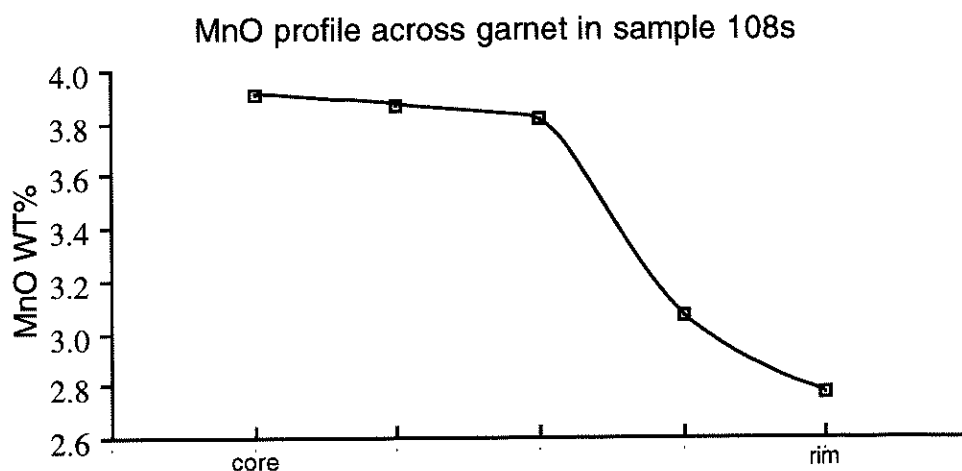


Greater profile differences are due to the high and probably rapid consumption of MnO by many garnet crystals in the early stages of crystalization. The MnO became

depleted from the matrix quickly (Graph 4k) as conditions for formation were favourable, so the garnet profile became depleted from the core to the rim in MnO. Crystal growth was relatively large (relative to samples 109, 105e and 111) due to the greater availability of MnO for garnet growth, but growth ceased due to the exhaustion of MnO by crystal development.

Sample 108s

Garnets were probed (Appendix D) that revealed MnO profiles which show a decrease in magnitude of MnO variation across the profile, similar to sample 108s. One garnet MnO profile (fig. 4l); 3.912-3.870-3.817-3.065-2.773, shows little variation in MnO across the profile. However the last value is complemented by an increase in CaO at this site.



Graph 4l Mno profile across garnet 108s, data in Appendix D

Sample 107a

Probe analyses for this sample were unavailable for discussion. Results from 107b are used for the construction of ternary diagrams, since it is the bulk composition variation that is important. The composition and assemblage proportions are similar to sample 107c, so assemblage development can be considered to be influenced by processes that created the assemblage in 107c.

SUMMARY

Appreciable differences are noticed between samples of this assemblage and those assemblages containing andalusite (section 4.2). Importantly the modal abundance of garnet increases with increasing bulk MnO contents. The distribution of the MnO within the garnet minerals is in accord with the inverse relationship outlined in the summary of the section above, and shown in graph 3. Garnets reveal "lower" MnO WT%`s in probe profiles, but occupied higher proportions of the samples. These lower values are due to the higher "competition" for MnO between the developing crystals. The fact that there is a greater difference between the rim and core values of the probe analyses implies that competition for MnO was high amongst the individual minerals.

The mineral assemblage is likewise described by the exhaustion of bulk MnO. Since Fe is incorporated into garnet before staurolite, staurolite growth was hampered till Mn was consumed to a level where garnet growth ceased. This decreased the competition for Fe, allowing for textures described in Appendix B to develop between minerals garnet, staurolite and andalusite.

CONCLUSION

Only from chemical analyses and petrological descriptions can the relationships between mineral assemblages be exposed, for small scale assemblages. Accurate sampling of the mineral assemblage and its corresponding composition provide data which permit the application of theoretical models, if these models are not sufficient for describing the minerals then further considerations must be made. The influence of neglected components must be incorporated into model systems to make them adequate for describing "real" rocks.

The failure of pseudo-sections (figs 4, 5 and 11) of Dymoke and Sandiford (1992) to describe the presence of garnet bearing pelitic rocks with garnet absent rocks is attributable to small amounts of MnO present in the systems, that was not accounted for in their calculations.

Projections of mineral assemblages onto AFM planes demonstrate the necessity for the involvement of neglected components. From bulk rock chemical analyses and petrology a relationship is observed between the component MnO and garnet. This relationship is highlighted by projections into the AFMn system, which clarify mineral assemblage conjectures that arise from AFM projections.

This relationship is exposed further from the comparison of MnO profiles across garnet crystals of selected samples. This demonstrates that small amounts of MnO are able to displace assemblage predictions for particular bulk Fe contents.

The data support predictions by Dymoke and Sandiford (1992) that the presence of small amounts of bulk MnO are able to stabilize garnet bearing rocks with garnet absent rocks.

Thus with the consideration of minor components and their proportions many small scale mineral assemblage relationships not described by models can be sufficiently described.

REFERENCES

- Deer, W.A., Howie, R.A. and Zussman, J., 1992. An Introduction to the Rock Forming Minerals. 2nd edition. Longman Scientific and Technical, Hong Kong.
- Dymoke, P. and Sandiford, M. 1992. Phase relationships in Buchan facies series pelitic assemblages: calculations with application to andalusite-staurolite parageneses in the Mount Lofty Ranges, South Australia. *Contrib. Min. Pet.*, **110**, p.121-132.
- Fleming, P.D., 1971. Metamorphism and folding in the Mt Lofty Ranges, South Australia, with particular reference to the Dawsley-Kanmantoo area. Ph.D. thesis, Univ. Adelaide (unpubl.).
- Holland, T.J.B. and Powell, R. 1990. An enlarged and updated internally consistent thermodynamic dataset with uncertainties and correlations: the system $K_2O-Na_2O-CaO-MgO-MnO-FeO-Fe_2O_3-Al_2O_3-TiO_2-SiO_2-C-H_2-O_2$. *J. Met. Geol.*, **8**, p.89-124.
- Howell, N.J., 1991. Calculated metapelitic mineral assemblages. Hons. Thesis. Univ. Melbourne (unpubl.).
- Jenkins, R.J.F. 1990. The Adelaide Fold Belt: Tectonic Reappraisal. In: J.B. Jago and P.S. Moore (Editors), *The Evolution of a Late PreCambrian to Early Palaeozoic Rift Complex: The Adelaide Geosyncline*. Geol. Soc. Aust. Spec. Publ., **16**: 215-229.
- Lindqvist, W. F. 1969. Geology and metamorphic history of the Kanmantoo Copper Deposit, South Australia. Ph.D. thesis (unpubl.).
- Marlow, P.C. and Etheridge, M.A., 1977. Development of a layered crenulation cleavage in mica schists of the Kanmantoo Group near Macclesfield, South Australia. *Geol. Soc. Amer. Bull.*, v.**88**, p.873- 882.
- Mancktelow, N. S. 1979. The structure and metamorphism of the Southern Adelaide Fold Belt, Ph.D. thesis, Univ. Adelaide (unpubl.).

- Manktelow, N.S.,1990. The structure of the Southern Adelaide Fold belt, south Australia.
In: J.B. Jago and P.S. Moore (Editors), The Evolution of a Late Precambrian-
Early Palaeozoic Rift Complex: The Adelaide Geosyncline. Geol. Soc. Aust.
Spec. Publ.,16: 215-229.
- Miriams, R.C. 1962. The geology of the Mt. Barker-Callington area. Mining Review, Sth.
Aust. Dept>Mines, **117**,pp.9-16.
- Offler,R. and Fleming, P.D., 1968. A synthesis of folding and metamorphism the Mt.
Lofty Ranges, South Aust. Journ. of the Geol. Society of Aust. 15, 245-266.
- Powell, R. and Holland, T.,1988. An internally consistent dataset with uncertainties and
correlations: Applications to geobarometry, worked examples and a computer
program *J. Met. Geol.* v.6, p173-204.
- Powell, R. and Holland, T.,1990. Calculated mineral equilibria in the pelite system,
KFMASH (K₂O-FeO-MgO-Al₂O₃-SiO₂-H₂O). *Amer. Min.*,v.75, p.367-380.
- Symmes, G.H. and Ferry, J.M. 1992. The effect of whole-rock MnO content on the
stability of garnet in pelitic in pelitic schists during metamorphism. *J. Met.
Geol.*, **10**, p.221-237.

FIGURES

Figure 1.

Jenkins, R.J.F. and Sandiford, M. 1992. Observations on the tectonic evolution of the
Southern Adelaide Fold Belt. *Tectonophysics*, 214.

Figure 2.

Offler,R. and Fleming, P.D., 1968. A synthesis of folding and metamorphism the Mt.
Lofty Ranges, South Aust. Journ. of the Geol. Society of Aust. 15, 245-266.

Figure 3.

Preiss, W.V., 1990. A stratigraphic and tectonic overview of the Adelaide Geosyncline, South Australia. In: J.B. Jago and P.S. Moore (Editors), *The Evolution of a Late Precambrian-Early Palaeozoic Rift Complex: The Adelaide Geosyncline*. Geol. Soc. Spec. Publ., 16: 1-33.

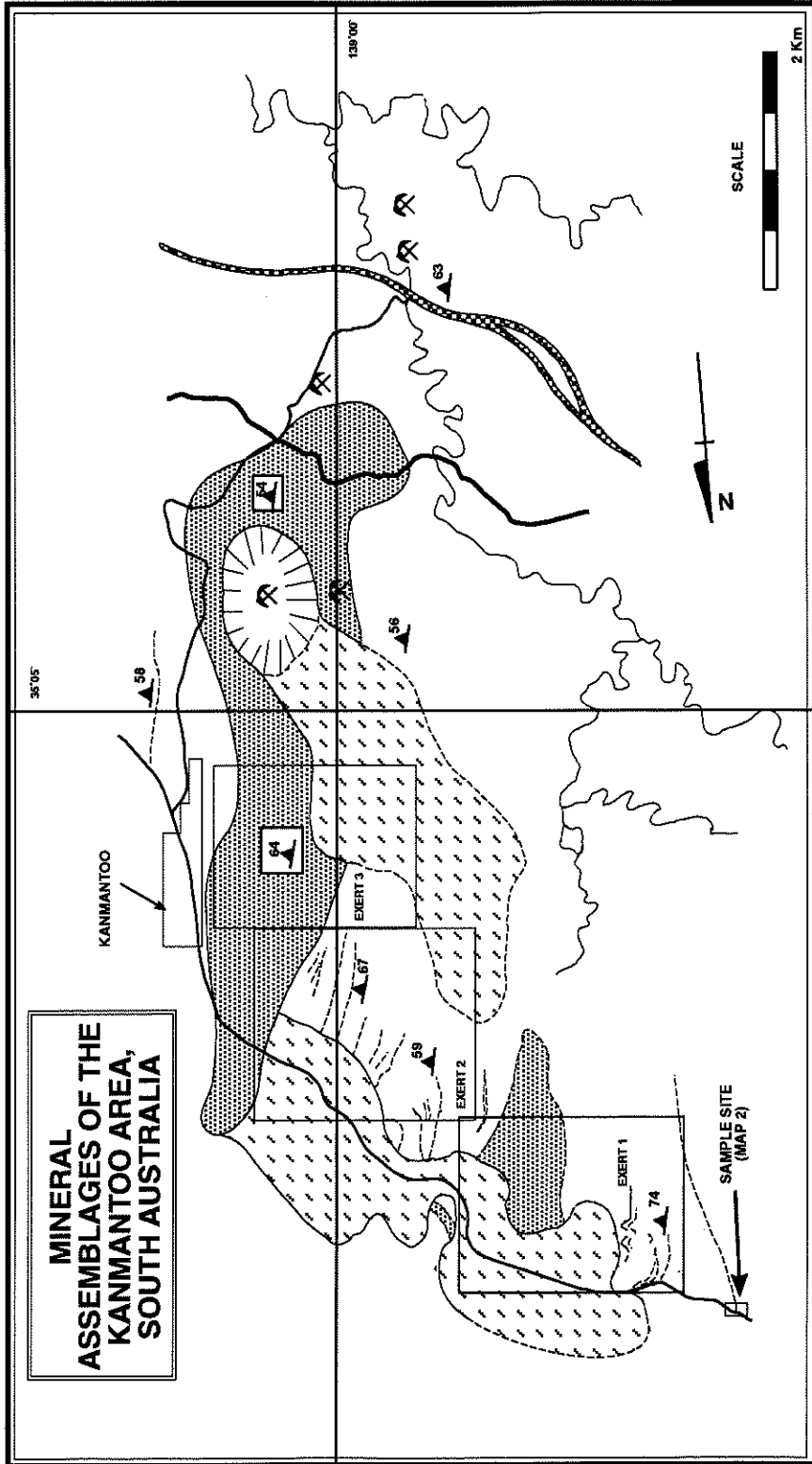
Figures 4, 5 and 11.

Dymoke, P. and Saandiford, M. 1992 Phase relationships in Buchan facies series pelitic assemblages: calculations with application to andalusite-staurolite parageneses in the Mount Lofty Ranges, South Australia. *Contrib. Min. Pet.*, **110**, p.121-132.

should be in main text.

Appendix A

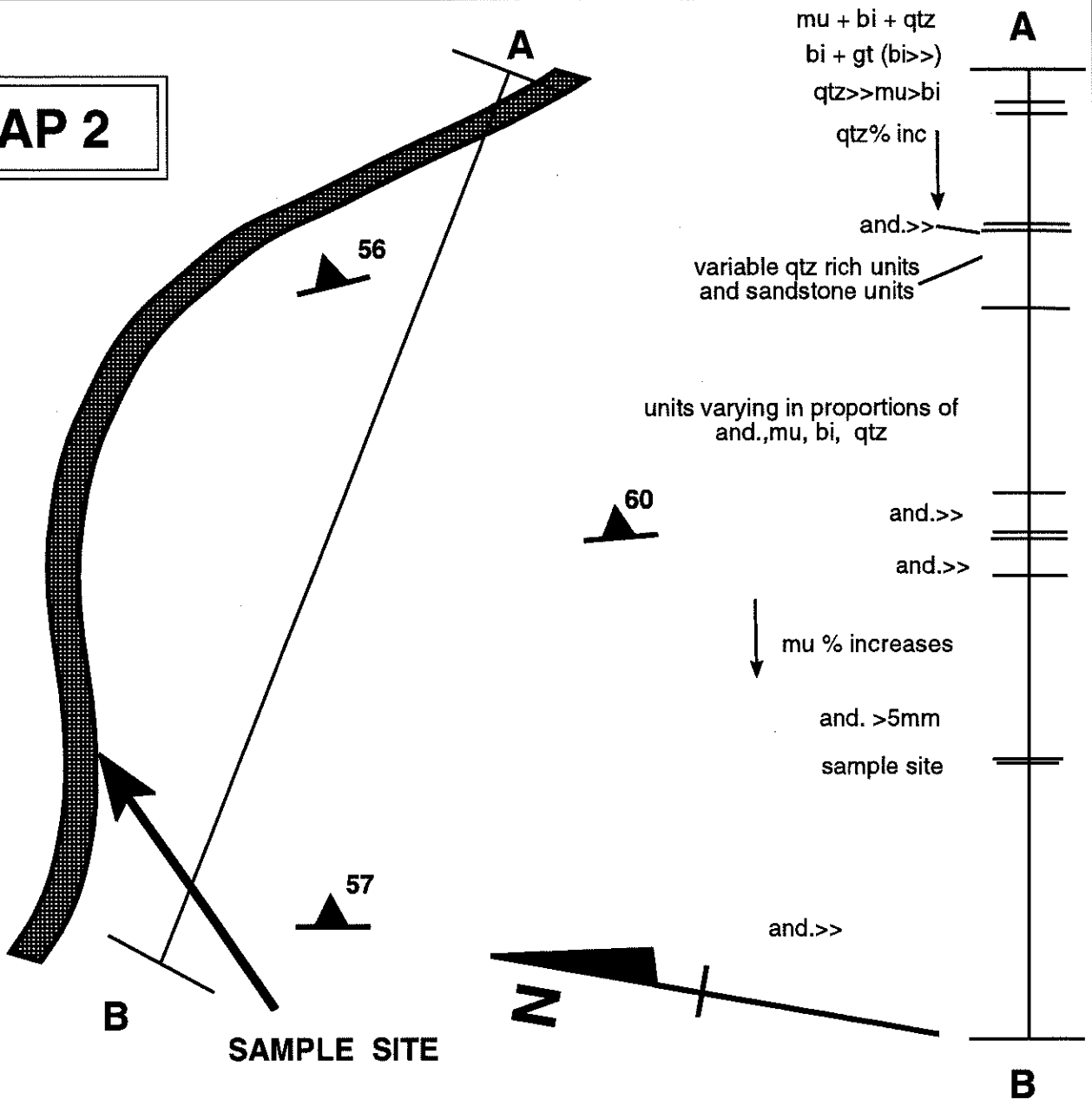
Maps are provided that show the location of the assemblages and their relationship to each other. Exerts from a general mineral assemblage map demonstrate the complexity of the mineral assemblages in the field. The difficulty of mapping these terrains is demonstrated by the exerts from Map 1. Outcrops appear far and distanced from each other in the field, making correlation of "continuous" outcrop over a large scale difficult.



MAP 1

Cross section of assemblages near sample site, showing broad variation in mineral proportions

MAP 2



**all assemblages
 +bi + mu + qtz
 (if not stated)**

LEGEND

SCALE

0 100m

PRINCES HIGHWAY
 Cleavage

SAMPLE SITE

MAP 3

**EAST
SIDE**

104 a

b

c

d

105 i

ii

e

106 a

b

107 a

b

c

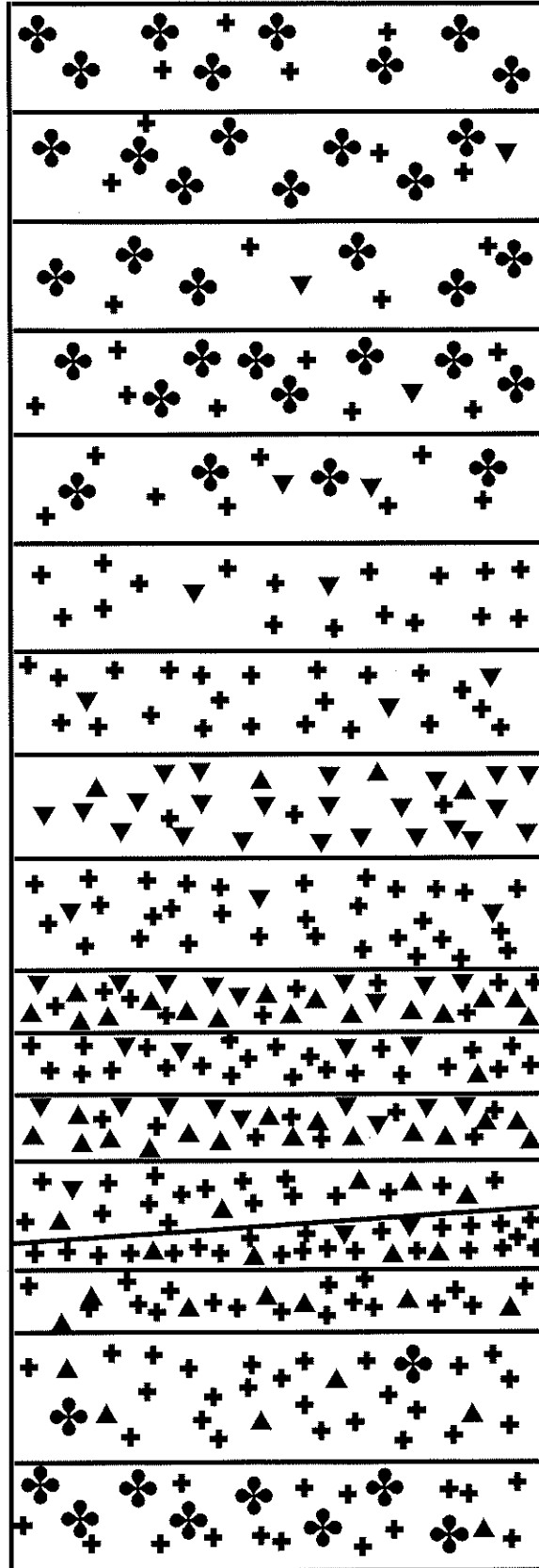
108

s

109

110

111



**KEY TO
MINERALS**



Andalusite



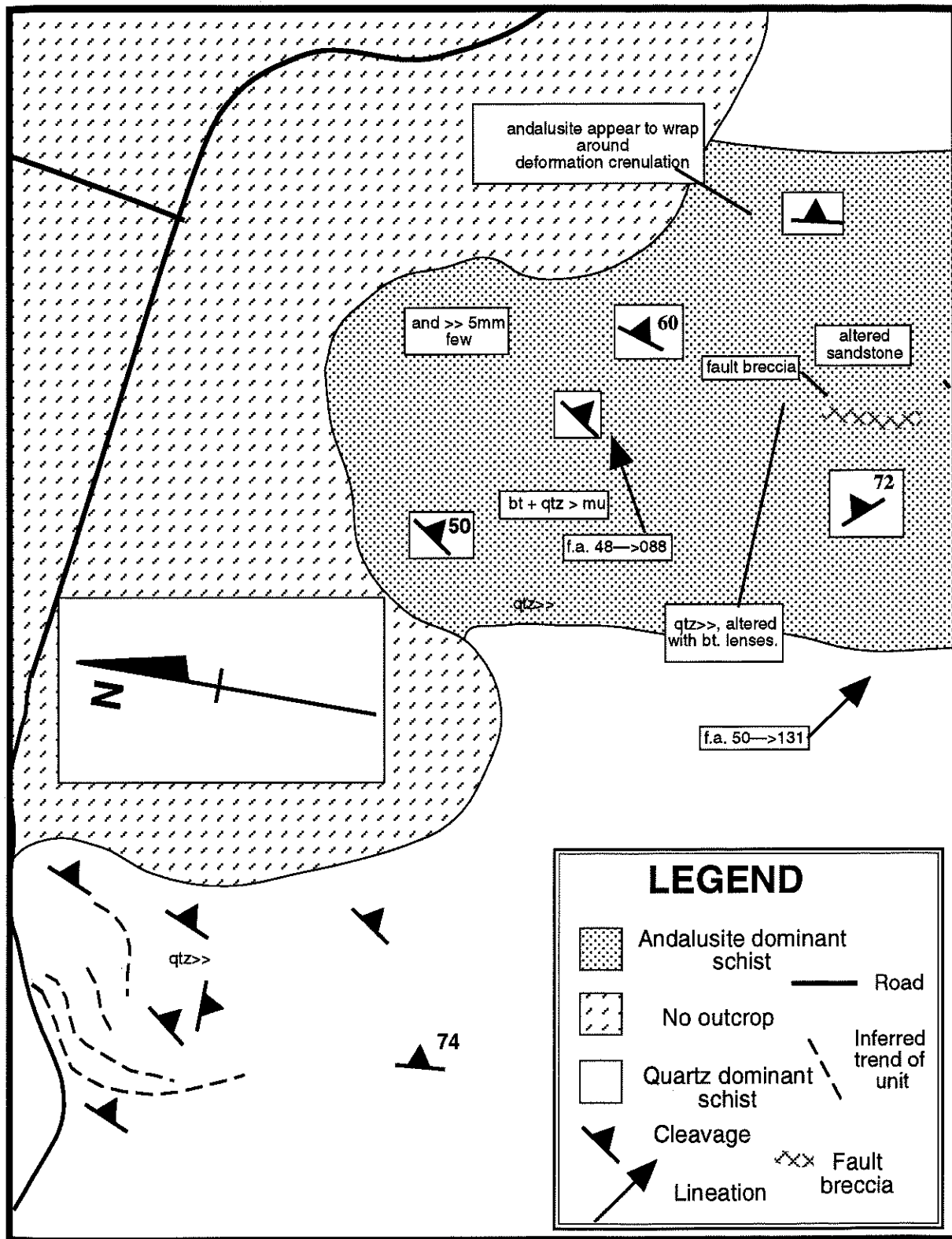
Garnet




Staurolite

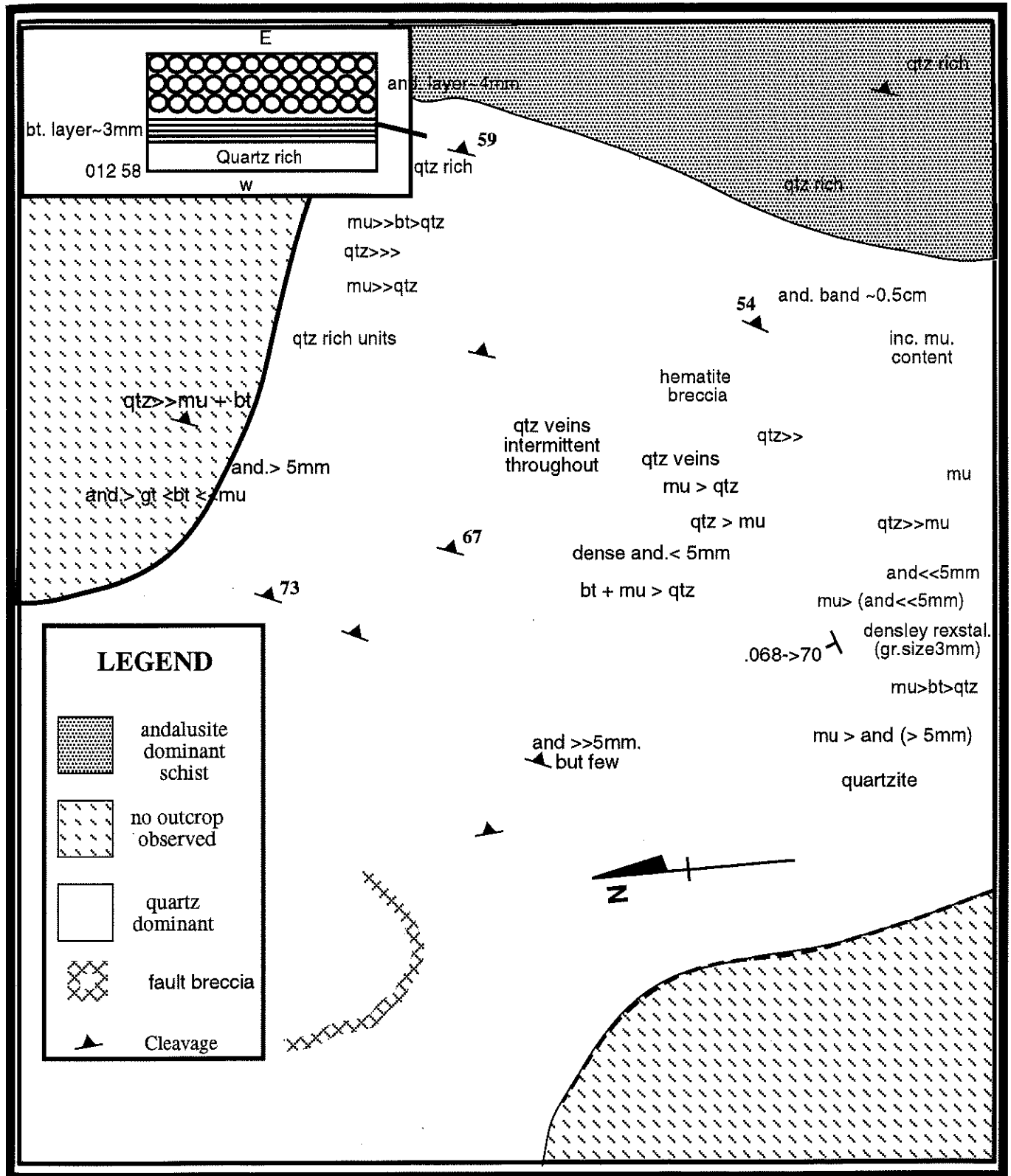
**WEST
SIDE**

Distribution of andalusite, staurolite and garnet across the sample space.

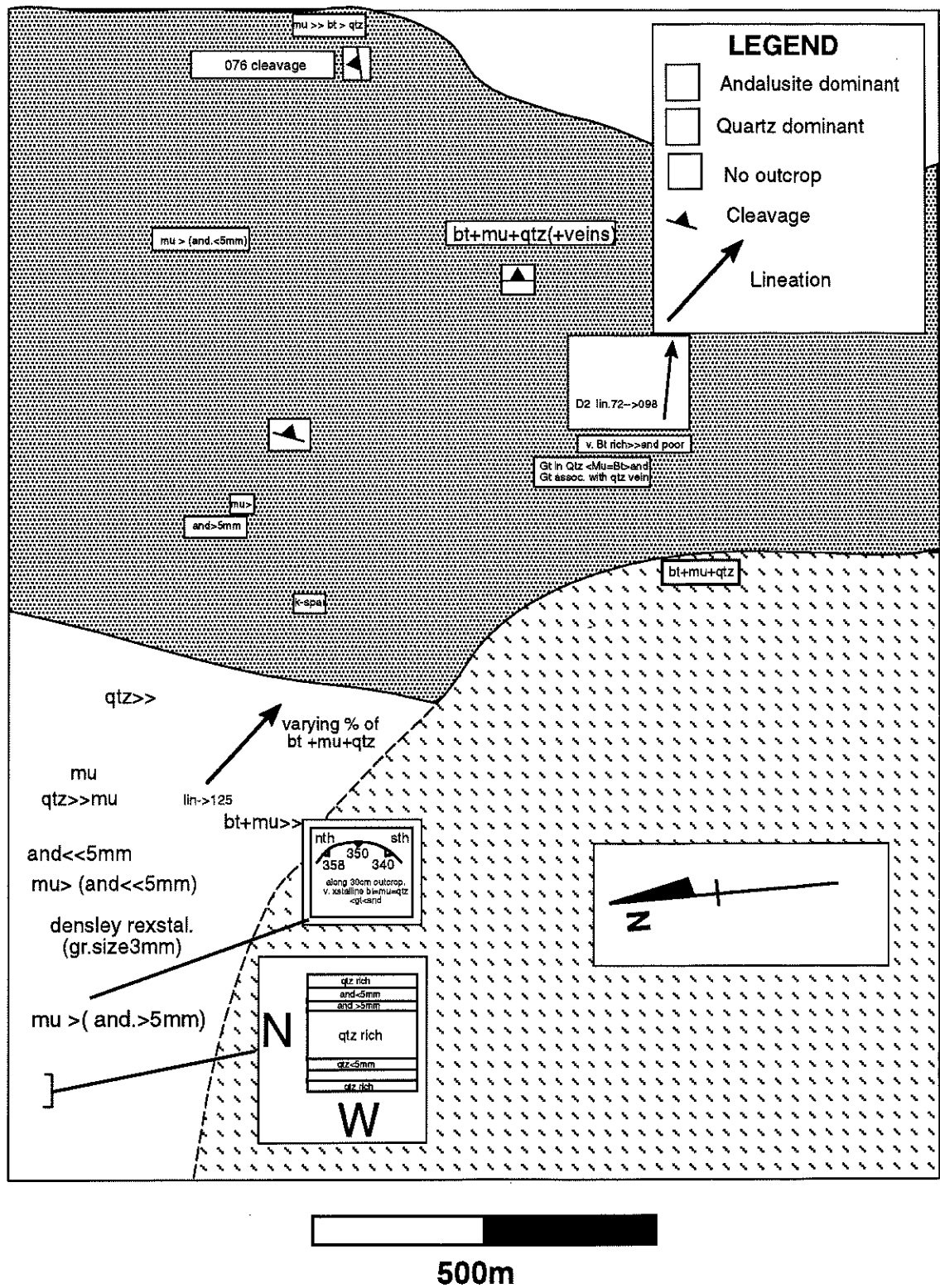


SCALE  500m

EXERT 1 Mineral assemblage diversification in the quartz rich units



EXERT 2 Mineral assemblage diversification in the quartz rich units



EXERT 3 Mineral assemblage diversification in the Kanmantoo Schists

APPENDIX B

PETROLOGY OF THE SAMPLES

The dominant mineral assemblage for the sample space is;

andalusite+staurolite+garnet+biotite+muscovite +quartz

The mineral proportions vary across the sample space in response to variable compositions, these proportions were calculated from point counting of solid mineral appearances.

The sample space is 60cm wide and was divided up into 18 different sections based upon mineral assemblage variations observed in the field. Petrological examination of samples as thin sections was essential for the determination of the equilibrium relationships between the minerals present (Appendix B).

Timing of the porphyroblast growth relative to previous deformation events can be observed in the mineral inclusion patterns.

General mineral relationships

The garnet phase can be seen to be texturally early, from comparison of the inclusion patterns contained within the boundaries of the minerals in the samples. The staurolite is the next mineral to appear, where it grows with the garnet. Andalusite is the last of the minerals to develop, this is indicated by the inclusion patterns that mimic the enveloping foliation.

SLIDE 104a

The minerals present are;
and st bi mu qtz.

The modal proportions of minerals present are;

andalusite≈20%

staurolite≈5%

quartz≈25%

biotite≈25%

muscovite≈25%

H.S. Light grey, fine quartz-biotite-muscovite matrix, with large (1.0cm) andalusite porphyroblasts and small (3mm) regular shaped staurolite crystals.

T.S. The andalusite and staurolite growth appear synchronous with deformation.

The staurolite appears to have grown first, since its inclusion patterns are slightly different to the surroundings. Whereas inclusion patterns in the andalusite are very similar to the cleavage giving the implication that cleavage controlled the porphyroblast growth. The size of andalusite are greater than 1cm.

SLIDE 104b

The minerals present are;
st and gt bi qtz.

The modal proportions of the minerals present are;

andalusite≈20%

staurolite≈5%

garnet≈1%

biotite≈20%

muscovite≈25%

quartz≈25%

opaques≈1-2%

H.S. Light grey, fine quartz-biotite-muscovite matrix, with large (1.5cm) andalusite porphyroblasts and staurolite (0.5 cm) crystals.

T.S. The garnet growth appears early and associated with the matrix, the andalusite and staurolite phases appear to have formed early in the deformation, since the biotite and muscovite matrix is folded around them. Late stage chlorite is observed to grow off of the andalusite rims, it is also observed to grow across the biotite-muscovite matrix, in no orientation. Late stage muscovite is seen to replace the andalusite.

SLIDE 104c

The minerals present are;

st and gt bi qtz.

The modal proportions of the minerals present are;

andalusite≈15%

staurolite≈5%

garnet≈1%

biotite≈25%

muscovite≈2%

quartz≈25%

H.S. Large andalusite (<1.0 cm) porphyroblasts dominate the sample, they are contained within a strongly foliated biotite matrix. Staurolite porphyroblasts (≈0.5cm) are distributed amongst the andalusite in random orientation.

T.S. Andalusite appears to be late stage mineral development since the inclusion patterns are similar to those of the surrounding matrix. The staurolite exhibit variable inclusion pattern morphologies indicating that growth occurred over a much longer period of deformation, and earlier in deformation. The garnet is "small" (>0.05cm) and located amongst the matrix, close to the andalusite porphyroblasts.

SLIDE 104d

The minerals present are;

st and gt bi qtz.

The modal proportions of the minerals present are;

andalusite≈20%

staurolite≈10%

garnet≈1%

quartz≈10%

biotite≈15%

muscovite≈40%

opaques≈3%

H.S. Andalusite (≈1.0cm) is the dominating porphyroblast in the sample section, staurolite (>0.7cm) is distributed amongst the andalusite. A quartz vein (late stage) cuts through the sample area but does not appear to have altered the minerals in any way. Garnet does not appear to be present, however thin-sections disprove this.

T.S. Like all samples of this series the fabric development demonstrates periods of intense deformation, with heavily crenulated to warped fabric. These periods of deformation are preserved in the developing porphyroblasts. The timing of the mineral growth is reflected in the textural relationships between the minerals, ie. garnet “inside” the boundaries of andalusite, or reside next to staurolites of different inclusion patterns.

SLIDE 105i

The minerals present are;

st and gt bi qtz.

The modal proportions of the minerals present are;

andalusite≈10%

staurolite≈10%

garnet≈4%

quartz≈55%

biotite≈7%

muscovite≈12%

H.S. The modal proportion and size of staurolite can be seen to increase relative to the previous samples. Andalusite porphyroblasts are still quite large, and garnet is not evident.

T.S. The andalusite porphyroblasts are replaced by a large percent of retrograde muscovite, the andalusite still exhibits inclusion patterns similar to the surrounding fabric. The staurolite, similar to the previous samples has variable inclusion patterns which represent its syn-deformational growth. Garnet is small (>0.05cm) and located in and amongst the rest of the mineral assemblage, often with either andalusite or staurolite.

SLIDE 105ii

The minerals present are;

st and gt bi qtz.

The modal proportions of the minerals present are;

staurolite≈25%

garnet≈5%

quartz≈30%

biotite≈25%

muscovite≈5%

H.S. The distinct lack of andalusite and the increase in staurolite in conjunction with the biotite make the appearance of this rock very different to those described before. It is a highly crenulated rock defined by biotite, in which crystals of staurolite and garnet have developed.

T.S. Many stages of growth are reflected by the variable inclusion patterns contained within the staurolite and garnet. The timing of growth, as outlined in the text, is a function of the bulk rock composition. Garnets have inclusion patterns oblique to the fabric, and at high angles to the inclusion patterns in

staurolite. This mineral growth reflects the bulk composition dependency as garnet develops early, before staurolite (as shown by its inclusion patterns).

SLIDE 105e

The minerals present are;

st and gt bi qtz.

The modal proportions of the minerals present are;

staurolite≈35%

andalusite≈5%

garnet≈6%

quartz≈25%

biotite≈25%

H.S. Very similar to the previous sample, except that there is a minor amount of andalusite present. Otherwise the rock is very dark (due to the biotite) and quite dense, the staurolite porphyroblasts appear randomly orientated amongst the fabric.

T.S. The staurolite growth was synchronous with late garnet growth, andalusite growth appears late. The timing of the andalusite growth can be gauged by the inclusions in the andalusite since they are all parallel to the external foliation. The garnet present appears associated with the matrix and not with other phases, the size of the garnet porphyroblasts is approximately 1mm, the andalusite size is about 5mm.

SLIDE 106a

The minerals present are;

g st bi qtz

Modal proportions of minerals present are;

staurolite≈5%

garnet≈40%

quartz≈25%

biotite≈25%

H.S. Appears as a dark highly “laminated” rock due to the intense biotite fabric development, the garnet which is nearly 1.5mm in diameter resides in between the biotite “laminations”. Biotite cleavage dominates the matrix of this sample, with quartz occurring between the biotite foliations, garnet appears associated with the biotite foliation. The minor amount of staurolite occurs in and amongst the matrix.

T.S. Staurolite growth appears early, with the inclusion morphology opposing that of the external foliation. The most distinguishing feature of this sample is the modal proportion of the garnet, which is greater than other samples. The sizes of garnet crystals range between 1.5mm and 2mm.

SLIDE 106b

The minerals present are

g st bi qtz mu

Modal proportions of the minerals are;

st≈40%

gt≈5%

qtz≈30%

bi≈20%

mu≈15%

H.S. Staurolite growth is most prolific in this sample, late stage biotite foliation is wrapped around the earlier formed porphyroblasts. Garnet is not seen in the hand specimen.

T.S. A number of different growth stages are observed for both the garnet and staurolite, which are defined by the inclusion morphologies of the minerals. Early phases recording inclusion patterns different to the present matrix foliation are seen, garnets that developed later contained inclusion patterns similar to the present foliation.

SLIDE 107a

The minerals present are;

g st bi qtz

The modal proportions of the minerals are;

staurolite≈20%

garnet≈40%

biotite≈25%

quartz≈20%

H.S. The rocks overall appearance is one of dissemination, where biotite fabric is “broken” up by the developing phases of garnet and staurolite. The garnet crystals become obvious in the hand specimen at this sample, as they reach sizes around 2mm. The staurolite does not appear “well” developed and is a reduced phase in this sample.

T.S. The garnet lack any inclusion patterns and appear morphologically different to those previously described, the staurolites contain minor inclusion patterns which reflect the stress field in which they developed. The mineral development appears to be confined along the biotite laminations and so the phases do not grow uncontrolled.

SLIDE 107b

The minerals present are;

g st bi qtz

The modal proportions of the minerals are;

staurolite≈35%

garnet≈15%

biotite≈20-25%

quartz≈20%

opaques≈5%

H.S. The hand specimen is very dark in colour, owing to the strong biotite fabric development and the garnet contained in the fabric. The distinguishing feature of this sample is the staurolite mineral contained in it, which is different to those previously discussed.

T.S. Late stage staurolite development has deformed the previously existing biotite fabric during its growth. Its growth occurred after the garnet formed and is separated from the garnet by the biotite fabric. A growth rim of biotite occurs inside the rim of the staurolite which indicates at least two phases of growth.

SLIDE 107c

The minerals present are;

g st bi qtz

The modal proportions of minerals are;

staurolite≈12%

garnet≈40%

quartz≈25%

biotite≈25%

H.S. Biotite foliation is a dominant feature of this sample, in which garnet appears to have grown, (a feature similar to 107a). Garnet appears large (2-2.5mm) and is quite visible in the hand specimen.

T.S. Garnet appears associated with the biotite foliation, which dominates the fabric of the rock. The garnet sizes are at their largest in the sample space, but seem to be confined by the biotite foliation. Chlorite and muscovite overgrow the matrix, the chlorite occurring with a radial texture.

SLIDE 108

The minerals present are;

g st bi qtz mu

The modal proportions of minerals are;

staurolite≈25%

garnet≈10%

quartz≈35%

biotite≈25%

muscovite≈10%

H.S. The staurolite and biotite are the most distinguishing features of this sample giving it its dark colour. Staurolite is contained in amongst the biotite-quartz fabric.

T.S. The staurolite shows variable inclusion patterns, often at completely different angles to the fabric owing to its syn-deformational development. The garnet appears texturally early in comparison to the staurolite interpreted from its inclusion pattern variation.

SLIDE 108s

The minerals present are;

g st bi qtz mu

The modal proportions of minerals are;

staurolite≈40%

garnet≈15%

quartz≈30%

biotite≈25%

H.S. Very similar to 108, however the staurolite crystals are much larger and deform the fabric to a greater extent.

T.S. The staurolite porphyroblasts exhibit variable inclusion patterns, so to do the garnets, this indicates syn-deformational growth. A number of crystals have inclusion patterns that are folded directly into the fabric, mimicking it identically. Garnet grew before the staurolite and were later enveloped by the staurolite as it grew, this is implied by garnets within the rims of staurolite.

SLIDE 109

The minerals present are;

st g bi qtz mu

The modal proportions of the minerals are;

staurolite≈35%

garnet≈15%

quartz≈25%

biotite≈15%

retro-mu≈10%

retro-chl?≈10%

H.S. Similar to samples 108 and 108s though the staurolite porphyroblasts are smaller, variable inclusion patterns are exhibited in the crystals, indicating syn-deformational growth. An alteration zone can be seen to cross cut the sample.

T.S. Morphology of the crystals is no different to those of samples 108 and 108s, except for the above mentioned alteration zone. This zone is noted on a large scale by Lindqvist (1969) as a chlorite alteration zone, in thin section this part is devoid of staurolite, late stage muscovite overgrows the matrix. The garnet size is about "average" (≈1mm), and has some inclusion patterns, though not indicative of early growth.

Garnet appears to have rims devoid of inclusion trails which implies later stages of growth. Reaction textures infer that some retrograde phases formed

at the expense of other phases. It appears as though late muscovite may have replaced andalusite porphyroblasts in places, and in doing so has adopted its poikiloblastic texture.

SLIDE 110

The minerals present are;

and g st bi mu qtz

The modal proportions of minerals are;

andalusite≈5%

staurolite≈15-20%

garnet≈5%

quartz≈25%

biotite≈25%

muscovite≈10%

feldspar≈5%

opaque≈1%

H.S. Appears similar to samples described before, however the presence of andalusite is noted

T.S. The andalusite appears has been overgrown by muscovite, this is possibly one of the transition stages in the formation of the porphyroblast of muscovite seen in the previous slide. Matrix muscovite is dominant in places, particularly between staurolite crystals, inferring that it was not consumed during phase production (reaction Chapter 3). Garnets appear to have nucleated in muscovite rich areas, some of these garnet are now included in staurolite.

Garnet displays distinct inclusion-free rims, which implies that the reaction producing staurolite changed in some way so that garnet continued to grow after its original formation. The modal proportions of muscovite, biotite and quartz vary throughout the matrix. Overall the proportions of muscovite

biotite and quartz are equivalent. The garnet sizes are around 1mm in diameter, andalusite porphyroblasts size is around 5mm across.

SLIDE 111

The minerals present are;

and + st + g + bi + qtz + mu + fsp

The modal proportions of minerals observed;

andalusite≈20%

staurolite≈25%

garnet≈2%

quartz≈20%

biotite≈20%

muscovite≈15%

potassium feldspar≈5%

H.S. The andalusite and staurolite assemblages comprise approximately 50% of the sample. The andalusite porphyroblasts occupy the greatest percentage of the slide. Quartz inclusions make-up over 70% of andalusite porphyroblasts. The andalusites are approximately 1cm in diameter and most of the staurolites≈5mm in diameter.

T.S. Garnet and feldspar appear amongst the matrix, many of the garnets bearing different inclusion patterns to the matrix foliation demonstrating syndeformational growth.

The garnet size is approximately 0.05mm, the andalusite size is 10mm

Appendix C

Electron Microprobe Analysis:

Seventeen ^othin sections were coated with approximately 250 microns of carbon for micro-probe analyses that were carried out using KEVEX 7000 Series energy dispersive system (E.D.S.) attached to a JEOL 733 Superprobe.

An accelerating voltage of 15KV and a beam current of 3nA were used during the analysis of the samples and each spectrum was collected over a 60sec time period. Callibration of the KEVEX EDS system was carried out using pure rhodonite sample.

Detection limits for the analysed elements are quite variable and depend upon several factors. The best estimate for all elements analysed is 0.1%.

Samples Analysed

sample 104a

sample 104b

sample 105i

sample 105e

sample 106a

sample 107c

sample 107b

sample 108

sample 108s

sample 109

sample 110

sample 111

	GARNET			GARNET			GARNET			STAUROLITE			MUSCOVITE			BIOTITE				
	rim1	tran1	core1	tran1	rim1	rim2	tran2	core2	tran2	rim2	rim	rim	rim	rim	rim					
SiO2	36.456	36.65	36.145	36.558	36.596	35.933	36.689	36.805	36.654	36.341	26.905	26.862	26.145	26.839	26.474	26.319	44.306	43.91	43.898	34.913
TiO2	0	0	0	0.204	0.11	0	0	0	0.061	0.057	0.654	0.506	0.616	0.52	0.715	0.746	0.737	0.621	0.337	1.501
Al2O3	21.304	21.239	21.63	21.475	21.755	21.739	21.703	21.719	21.689	21.611	52.545	52.607	52.727	52.66	52.985	51.844	35.445	35.115	35.875	19.517
FeO	32.358	32.125	31.977	32.317	33.137	33.241	32.369	32.719	33.003	33.58	14.642	14.092	14.364	14.597	14.31	13.764	0.656	0.426	0.648	20.19
MnO	5.167	5.223	5.469	5.284	5.134	5.1	5.366	5.296	5.37	5.144	0.29	0.366	0.549	0.157	0.403	0.435	0	0.007	0.057	0.327
MgO	2.607	2.354	2.347	2.813	2.394	2.545	2.318	2.659	2.72	2.083	1.112	1.24	1.017	1.252	1.353	1.172	0.166	0.217	0.39	9.33
CaO	1.337	1.705	1.695	1.74	1.493	1.518	1.851	1.691	1.614	1.521	0.234	0.038	0.139	0.047	0	0.034	0.256	0.106	0.108	0.198
Na2O	0.045	0.304	0	0.243	0.009	0.451	0	0.177	0.003	0.273	0.127	0	0.036	0	0	0.045	1.088	1.281	1.325	0
K2O	0	0	0	0	0.088	0.03	0.059	0	0	0	0.023	0	0	0	0	0	9.15	8.863	8.589	8.814
TOTAL	99.274	99.6	99.263	100.63	100.72	100.56	100.36	101.07	101.11	100.61	96.532	95.711	95.593	96.072	96.24	94.359	91.804	90.546	91.227	94.79
Si	2.9682	2.976	2.946	2.9404	2.9449	2.9075	2.9578	2.9481	2.9384	2.9381	7.9595	7.9838	7.8124	7.9601	7.8419	7.938	3.0391	3.0465	3.0219	2.6763
Ti	0	0	0	0.0123	0.0067	0	0	0	0.0037	0.0035	0.1455	0.1131	0.1384	0.116	0.1593	0.1692	0.038	0.0324	0.0174	0.0865
Al	2.0449	2.0332	2.0784	2.0363	2.0639	2.0737	2.0627	2.051	2.0498	2.0599	18.326	18.433	18.575	18.413	18.503	18.434	2.8664	2.8722	2.9115	1.7638
Fe 2+	2.2033	2.1816	2.1797	2.1739	2.2301	2.2494	2.1824	2.1918	2.2127	2.2706	3.6227	3.5028	3.5896	3.6207	3.545	3.4719	0.0376	0.0247	0.0373	1.2944
Mn	0.3563	0.3593	0.3776	0.36	0.3499	0.3495	0.3664	0.3593	0.3646	0.3523	0.0727	0.0921	0.139	0.0394	0.1011	0.1111	0	0.0004	0.0033	0.0212
Mg	0.3163	0.2849	0.2851	0.3372	0.2871	0.3069	0.2785	0.3174	0.325	0.251	0.4903	0.5493	0.4529	0.5534	0.5973	0.5268	0.017	0.0224	0.04	1.0659
Ca	0.1166	0.1483	0.148	0.15	0.1287	0.1316	0.1599	0.1451	0.1386	0.1318	0.0742	0.0121	0.0445	0.0149	0	0.011	0.0188	0.0079	0.008	0.0163
Na	0.0071	0.0479	0	0.0379	0.0014	0.0708	0	0.0275	0.0005	0.0428	0.0729	0	0.0209	0	0	0.0263	0.1447	0.1723	0.1769	0
K	0	0	0	0	0.009	0.0031	0.0061	0	0	0	0.0087	0	0	0	0	0	0.8007	0.7845	0.7543	0.862
TOTAL	8.0129	8.0313	8.0148	8.048	8.0217	8.0926	8.0139	8.0402	8.0333	8.0499	30.773	30.686	30.772	30.717	30.747	30.689	6.9624	6.9634	6.9705	7.7863

Selected probe data for sample 111

	BIOTITE			GARNET			STAUROLITE			MUSCOVITE			
	core1	rim1	rim1	rim	rim	rim	rim	rim	tran	core	rim	rim	core
SiO2	35.022	40.215	34.087	35.834	35.894	36.392	26.621	26.963	27.045	26.986	26.474	26.319	26.221
TiO2	1.861	1.306	1.548	0.125	0.127	0	0.466	0.568	0.528	0.55	0.715	0.746	0.612
Al2O3	19.939	19.745	19.709	21.025	21.562	21.606	52.829	53.342	53.32	53.04	52.985	51.844	52.768
FeO	20.261	16.909	19.489	33.296	32.834	33.43	14.516	14.592	13.392	14.572	14.31	13.764	13.794
MnO	0.186	0.283	0.009	5.198	6.175	5.443	0.372	0.568	0.309	0.372	0.403	0.435	0.397
MgO	9.046	7.708	9.312	2.306	1.844	1.991	1.338	1.346	1.276	1.272	1.353	1.172	1.534
CaO	0.227	0.118	0.263	1.512	1.518	1.72	0.166	0.125	0.171	0	0	0.034	0.043
Na2O	0	0.619	0.238	0.216	0	0	0	0	0.067	0.178	0	0.045	0.039
K2O	8.64	6.619	8.431	0.025	0	0	0	0	0	0	0	0	0
TOTAL	95.182	93.522	93.086	99.537	99.954	100.58	96.308	97.504	96.108	96.97	96.24	94.359	95.408
Si	2.6671	2.9864	2.6512	2.9338	2.9267	2.9433	7.8881	7.8948	7.9746	7.9388	7.8419	7.938	7.8213
Ti	0.1066	0.0729	0.0905	0.0077	0.0078	0	0.1038	0.1251	0.1171	0.1217	0.1593	0.1692	0.1373
Al	1.7902	1.7286	1.8072	2.0294	2.0726	2.0601	18.455	18.413	18.535	18.395	18.503	18.434	18.556
Fe 2+	1.2904	1.0501	1.2677	2.2799	2.239	2.2612	3.5972	3.5732	3.3025	3.5852	3.545	3.4719	3.4411
Mn	0.012	0.0178	0.0006	0.3605	0.4265	0.3729	0.0934	0.1409	0.0772	0.0927	0.1011	0.1111	0.1003
Mg	1.0267	0.8531	1.0794	0.2814	0.2241	0.24	0.5909	0.5874	0.5607	0.5577	0.5973	0.5268	0.6819
Ca	0.0185	0.0094	0.0219	0.1326	0.1326	0.1491	0.0527	0.0392	0.054	0	0	0.011	0.0137
Na	0	0.0891	0.0359	0.0343	0	0	0	0	0.0383	0.1015	0	0.0263	0.0226
K	0.8395	0.6271	0.8366	0.0026	0	0	0	0	0	0	0	0	0
TOTAL	7.7509	7.4345	7.7909	8.0622	8.0292	8.0266	30.781	30.774	30.66	30.793	30.747	30.689	30.775
							90.177	89.551	91.227	90.945			
							3.0261	3.037	3.0219	3.0841			
							0.0432	0.0187	0.0174	0.0301			
							2.873	2.8657	2.9115	2.8108			
							0.0201	0.0285	0.0373	0.0399			
							0.006	0.0058	0.0033	0			
							0.0366	0.0559	0.04	0.04			
							0.0191	0.0167	0.008	0.0024			
							0.1544	0.145	0.1769	0.1562			
							0.7857	0.8214	0.7543	0.7899			
TOTAL	6.9642	6.9947	6.9705	6.9534									

Selected probe data for sample 110

OXIDE	BIOTITE				GARNET				GARNET				STAUROLITE				MUSCOVITE			
	rim1	tran1	core1	tran1	rim1	tran2	core2	tran2	rim2	tran2	core2	tran2	rim2	rim	rim	rim	mu			
34.272	34.843	34.403	34.038	35.331	36.024	36.86	36.054	36.386	35.445	36.577	36.824	36.085	36.016	35.6	36.039	27.226	26.331	26.636	46.342	
1.49	1.887	1.503	2.335	1.262	0.034	0.194	0.09	0	0	0.012	0.0113	0.037	0.206	0.098	0.101	0.611	0.491	0.709	0.146	
19.884	19.998	19.232	19.702	20.755	21.496	21.524	21.666	21.45	21.49	21.533	21.394	21.322	21.241	21.392	21.268	53.552	52.783	53.128	31.19	
19.26	19.286	18.668	18.98	18.716	31.974	31.439	31.496	31.065	31.713	32.206	31.291	30.248	30.805	31.206	31.725	12.942	13.988	12.774	1.967	
0.156	0.341	0.249	0.119	0.052	6.343	6.752	6.978	6.391	6.597	7.321	6.869	7.158	6.782	6.897	6.788	0.393	0.48	0.508	0	
9.292	9.423	9.259	9.443	9.706	2.455	2.421	2.742	2.527	2.567	2.07	2.18	2.766	2.548	2.79	2.517	1.261	1.344	1.304	0.738	
0.179	0.26	0.204	0.115	0.077	1.421	1.428	1.719	1.396	1.505	1.504	1.449	1.423	1.674	1.46	1.5	0.131	0.094	0.208	0.155	
0	0	0	0	0.052	0	0	0	0	0.123	0	0.04	0.043	0.075	0.001	0	0.008	0	0.322	0.004	
8.618	9.001	8.402	8.622	8.386	0	0.022	0	0	0	0	0	0	0.002	0.002	0	0	0.095	0	9.931	
TOTAL	93.151	95.039	91.92	93.354	94.337	99.747	100.64	100.75	99.215	99.44	101.22	100.06	99.082	99.349	99.446	99.938	96.124	95.596	95.589	90.473
Si	2.66	2.6548	2.6978	2.6349	2.682	2.9326	2.9638	2.9088	2.963	2.9021	2.9442	2.9792	2.9461	2.9385	2.9092	2.9324	8.0049	7.85	7.8979	3.2405
Ti	0.087	0.1081	0.0886	0.1359	0.072	0.0021	0.0117	0.0055	0	0	0.0007	0.0007	0.0023	0.0126	0.006	0.0062	0.1351	0.1101	0.1581	0.0077
Al	1.8194	1.7963	1.7779	1.798	1.8574	2.063	2.0404	2.0608	2.0593	2.0744	2.0434	2.0405	2.0523	2.0431	2.061	2.0401	18.562	18.552	18.572	2.5712
Fe2+	1.2502	1.2289	1.2243	1.2288	1.1882	2.1769	2.1142	2.1252	2.1157	2.1716	2.168	2.1172	2.0654	2.102	2.1328	2.1589	3.1824	3.4877	3.1677	0.115
Mn	0.0103	0.022	0.0165	0.0078	0.0033	0.4374	0.4599	0.4769	0.4408	0.4575	0.4992	0.4707	0.495	0.4687	0.4774	0.4678	0.0979	0.1212	0.1276	0
Mg	1.0748	1.07	1.0821	1.0894	1.0981	0.2978	0.2901	0.3297	0.3067	0.3132	0.2483	0.2628	0.3366	0.3098	0.3398	0.3052	0.5525	0.5972	0.5762	0.0769
Ca	0.0149	0.0212	0.0171	0.0095	0.0063	0.124	0.123	0.1486	0.1218	0.132	0.1297	0.1256	0.1245	0.1463	0.1278	0.1308	0.0413	0.03	0.0661	0.0116
Na	0	0	0	0	0.0077	0	0	0	0	0.0195	0	0.0063	0.0068	0.0119	0.0002	0	0.0046	0	0.1851	0.0005
K	0.8534	0.875	0.8406	0.8515	0.8122	0	0.0023	0	0	0	0	0	0	0.0002	0.0002	0	0	0.0323	0	0.886
TOTAL	7.77	7.7764	7.7449	7.7559	7.7271	8.0338	8.0054	8.0554	8.0073	8.0704	8.0334	8.003	8.0289	8.0333	8.0544	8.0414	30.581	30.78	30.751	6.9095

Selected probe data for sample 109

	GARNET				GARNET				STAUROLITE				BIOTITE		
	core1	tran1	tran1	rim1	core2	tran2	rim2	rim2	rim	rim	rim	rim	rim	rim	rim
SiO2	36.394	35.781	36.413	36.73	36.976	36.882	36.271	34.171	34.133	27.069	27.352	34.217	34.217		
TiO2	0.011	0	0.112	0	0.122	0.131	0.045	0.03	0.615	0.722	0.561	1.488	1.488		
Al2O3	21.591	21.782	21.964	21.617	21.493	21.592	21.325	20.008	51.999	53.936	53.209	23.786	23.786		
FeO	34.263	34.4	35.007	35.983	35.387	34.199	34.221	35.435	11.714	13.18	15.135	16.981	16.981		
MnO	3.912	3.87	3.817	3.065	2.773	4.14	3.991	2.951	0.208	0.158	0.256	0.226	0.226		
MgO	2.432	2.311	2.638	2.568	2.366	2.407	2.369	1.735	1.194	1.348	1.394	8.706	8.706		
CaO	1.899	1.961	1.83	1.388	1.511	1.993	1.92	1.675	0.213	0.026	0.072	0.105	0.105		
Na2O	0	0	0.213	0.228	0.321	0	0	0	0	0.104	0	0.061	0.061		
K2O	0.002	0	0.004	0.032	0	0	0.124	0.065	0.318	0	0	7.191	7.191		
	100.5	100.11	102	101.62	100.95	101.34	100.26	96.07	100.39	96.543	97.979	92.761	92.761		
Si	2.9387	2.9076	2.9044	2.9396	2.9671	2.951	2.9413	2.9221	9.4524	7.9276	7.9728	2.8345	2.8345		
Ti	0.0007	0	0.0067	0	0.0074	0.0079	0.0027	0.0019	0.1281	0.159	0.123	0.0927	0.0927		
Al	2.0553	2.0867	2.0654	2.0396	2.0333	2.0368	2.0387	2.0171	16.977	18.622	18.285	2.3229	2.3229		
Fe 2+	2.3138	2.3378	2.3352	2.4091	2.3748	2.2885	2.3209	2.5343	2.713	3.2282	3.6896	1.1764	1.1764		
Mn	0.2676	0.2664	0.2579	0.2078	0.1885	0.2806	0.2735	0.2138	0.0488	0.0392	0.0632	0.0159	0.0159		
Mg	0.2927	0.2799	0.3136	0.3063	0.2829	0.287	0.2863	0.2211	0.4928	0.5884	0.6056	1.0748	1.0748		
Ca	0.1643	0.1707	0.1564	0.119	0.1299	0.1709	0.1668	0.1535	0.0632	0.0082	0.0225	0.0093	0.0093		
Na	0	0	0.0329	0.0354	0.0499	0	0	0	0	0.0591	0	0.0098	0.0098		
K	0.0002	0	0.0004	0.0033	0	0	0.0128	0.0071	0.1124	0	0	0.76	0.76		
TOTAL	8.0331	8.0491	8.0729	8.06	8.0339	8.0227	8.043	8.0709	29.987	30.632	30.762	8.2963	8.2963		

	GARNET				GARNET				STAUROLITE			
	rim1	tran1	core1	tran1	rim1	rim2	tran2	core2	tran2	rim2	rim	st
SiO2	36.079	36.112	35.36	36.005	36.578	36.435	36.442	37.034	36.426	36.674	26.728	27.003
TiO2	0.151	0	0.02	0.029	0.007	0.02	0	0.102	0.044	0.009	0.434	0.557
Al2O3	21.222	21.42	21.319	21.169	21.398	21.517	21.437	21.393	21.226	21.877	52.632	53.693
FeO	35.631	33.883	33.611	34.558	36.281	36.736	35.5	34.081	34.325	35.663	14.631	13.765
MnO	3.115	3.685	3.369	3.478	2.643	2.574	2.537	2.967	2.834	2.724	0.358	0.06
MgO	2.548	2.178	2.303	2.233	2.187	2.115	2.683	2.439	2.406	2.112	1.592	0.902
CaO	1.524	1.951	2.056	1.941	1.319	1.289	1.812	1.83	1.849	1.635	0.235	0.124
Na2O	0.013	0	0.402	0.011	0	0.157	0.136	0.155	0	0.104	0.107	0.189
K2O	0.037	0.048	0	0	0	0	0	0.036	0	0	0	0
TOTAL	100.32	99.277	98.44	99.424	100.41	100.84	100.55	100.04	99.11	100.8	96.717	96.293
Si	2.9289	2.9493	2.9175	2.9441	2.9606	2.9435	2.9408	2.9859	2.971	2.95	7.8974	7.951
Ti	0.0092	0	0.0012	0.0018	0.0004	0.0012	0	0.0062	0.0027	0.0005	0.0964	0.1233
A	2.0311	2.0624	2.0737	2.0407	2.0418	2.0493	2.0394	2.0334	2.041	2.0746	18.334	18.639
Fe 2+	2.4191	2.3144	2.3193	2.3633	2.4559	2.462	2.3959	2.298	2.3414	2.3992	3.6155	3.3897
Mn	0.2142	0.2549	0.2355	0.2409	0.1812	0.1761	0.1734	0.2026	0.1958	0.1856	0.0896	0.015
Mg	0.3083	0.2651	0.2832	0.2721	0.2638	0.2546	0.3227	0.2931	0.2925	0.2532	0.701	0.3958
Ca	0.1326	0.1707	0.1818	0.1701	0.1144	0.1116	0.1567	0.1581	0.1616	0.1409	0.0744	0.0391
Na	0.002	0	0.0643	0.0017	0	0.0246	0.0213	0.0242	0	0.0162	0.0613	0.1079
K	0.0038	0.005	0	0	0	0	0	0.0037	0	0	0	0
total	8.0493	8.0219	8.0765	8.0347	8.0181	8.043	8.0501	8.0052	8.0059	8.0203	30.87	30.66

Selected probe data for sample 108

	GARNET				BIOTITE				STAUFOLITE				
	core	core	rim	rim	rim	rim	rim	rim	rim	rim	rim	rim	rim
SiO2	35.919	35.423	36.064	36.299	35.177	36.918	34.308	33.956	35.033	26.678	26.792	26.597	
TiO2	0.255	0.217	0.071	0.116	0.029	0.131	1.645	1.457	1.314	0.528	0.34	0.122	
Al2O3	19.013	19.005	19.095	19.863	18.923	19.577	17.13	17.48	17.875	48.523	48.175	47.779	
FeO	33.225	32.942	35.316	35.738	34.566	35.735	21.166	18.339	18.116	14.16	14.846	14.462	
MnO	5.922	5.946	3.976	2.855	3.031	2.783	0	0.058	0	0.477	0.185	0.134	
MgO	1.545	1.222	1.756	1.865	1.907	1.889	7.108	7.466	7.317	0.903	1.115	1.375	
CaO	2.08	2.249	2.082	1.832	1.435	1.332	0.169	0.178	0.358	0.006	0.171	0.052	
Na2O	0.008	0.36	0.16	0.184	0.861	0	0	0.128	0	0	0.263	0.151	
K2O	0.006	0.143	0	0	0	0	8.804	8.382	9.075	0	0	0	
TOTAL	97.973	97.507	98.52	98.752	95.929	98.365	90.33	87.444	89.088	91.275	91.887	90.672	
Si	3.0102	2.9927	3.0072	3.0014	3.0033	3.0524	2.7857	2.8044	2.836	8.3392	8.3529	8.3809	
Ti	0.0161	0.0138	0.0045	0.0072	0.0019	0.0081	0.1005	0.0905	0.08	0.1241	0.0797	0.0289	
Al	1.8785	1.8929	1.8772	1.9363	1.9047	1.9082	1.6398	1.702	1.706	17.882	17.707	17.749	
Fe 2+	2.3287	2.3276	2.4629	2.4714	2.4681	2.471	1.4373	1.2667	1.2265	3.7018	3.8709	3.8112	
Mn	0.4204	0.4255	0.2808	0.2	0.2192	0.1949	0	0.0041	0	0.1263	0.0489	0.0358	
Mg	0.193	0.1539	0.2182	0.2298	0.2426	0.2328	0.8601	0.9189	0.8828	0.4207	0.5181	0.6457	
Ca	0.1868	0.2036	0.186	0.1623	0.1313	0.118	0.0147	0.0158	0.0311	0.002	0.0571	0.0176	
Na	0.0013	0.059	0.0259	0.0295	0.1425	0	0	0.0205	0	0	0.159	0.0923	
K	0.0006	0.0154	0	0	0	0	0.912	0.8832	0.9373	0	0	0	
total	8.0355	8.0843	8.0627	8.0379	8.1137	7.9854	7.75	7.706	7.6996	30.596	30.793	30.762	

Selected probe data for sample 107b.

	BIOTITE						GARNET						GARNET						STAUROLITE					
	rim1	tran1	core1	tran1	rim1	rim2	tran2	core2	rim1	tran1	core1	tran1	rim1	tran1	core1	rim2	tran2	core2	rim1	tran	core			
SiO2	34.909	34.785	33.525	33.24	36.263	36.917	25.639	36.58	36.649	36.82	36.188	36.607	35.863	28.109	27.499	27.15	26.923							
TiO2	1.495	1.596	1.417	1.895	1.15	0.056	0.037	0.05	0.078	0	0	0.05	0	0.5	0.475	0.486	0.576							
Al2O3	20.97	21.154	19.722	20.557	21.098	21.393	15.752	21.787	21.197	22.003	21.175	21.442	21.143	52.341	54.926	53.649	53.034							
FeO	19.962	20.405	18.181	17.998	17.413	36.279	38.136	36.609	36.334	36.606	36.339	35.835	35.429	13.206	14.364	13.958	15.081							
MnO	0.115	0	0.062	0.196	0.163	2.359	1.199	2.08	2.15	2.243	2.275	2.888	3.019	0.19	0.319	0.183	0.256							
MgO	7.888	8.344	8.25	7.617	6.895	2.258	1.239	2.512	2.324	2.442	2.441	2.406	2.125	2.123	1.078	1.66	1.438							
CaO	0.268	0.23	0.288	0.231	0.299	1.981	1.113	1.484	1.45	1.682	1.447	1.841	2.476	0.147	0.046	0.06	0.05							
Na2O	0.094	0.298	0	0.068	0	0.1	0.261	0	0.063	0	0.204	0.048	0.064	0.309	0.244	0.046	0							
K2O	8.817	8.147	8.575	7.558	6.675	0.038	0	0.038	0.012	0	0.016	0.011	0	0.538	0	0	0							
TOTAL	94.518	94.959	90.02	89.36	89.956	101.38	83.376	101.14	100.26	101.8	100.09	101.13	100.12	97.463	98.951	97.192	97.358							
Si	2.6722	2.6459	2.6842	2.6614	2.8266	2.9593	2.6663	2.9362	2.9676	2.9357	2.9434	2.9436	2.9239	8.1921	7.903	7.9311	7.9029							
Ti	0.0861	0.0913	0.0853	0.1141	0.0674	0.0034	0.0029	0.003	0.0048	0	0	0.003	0	0.1096	0.1027	0.1068	0.1272							
Al	1.8924	1.897	1.8616	1.9404	1.9388	2.0217	1.9312	2.0617	2.0235	2.0682	2.0305	2.0327	2.0322	17.984	18.61	18.476	18.353							
Fe 2+	1.278	1.2981	1.2174	1.2052	1.1351	2.4322	3.3168	2.4576	2.4606	2.4409	2.4719	2.4099	2.4158	3.2188	3.4524	3.4101	3.7023							
Mn	0.0075	0	0.0042	0.0133	0.0108	0.1602	0.1056	0.1414	0.1475	0.1515	0.1567	0.1967	0.2085	0.0469	0.0777	0.0453	0.0637							
Mg	0.8999	0.9459	0.9844	0.9089	0.801	0.2698	0.192	0.3005	0.2605	0.2902	0.2959	0.2883	0.2582	0.9221	0.4617	0.7227	0.6291							
Ca	0.022	0.0187	0.0247	0.0198	0.025	0.1702	0.124	0.1276	0.1258	0.1437	0.1261	0.1586	0.2163	0.0459	0.0142	0.0188	0.0157							
Na	0.014	0.044	0	0.0106	0	0.0155	0.0526	0	0.0099	0	0.0322	0.0075	0.0101	0.1746	0.136	0.0261	0							
K	0.8611	0.7906	0.8759	0.772	0.6638	0.0039	0	0.0039	0.0012	0	0.0017	0.0011	0	0.2	0	0	0							
total	7.733	7.7315	7.7377	7.6456	7.4685	8.0361	8.3915	8.0319	8.0214	8.0302	8.0583	8.0414	8.065	30.894	30.757	30.737	30.794							

Selected probe data for sample 107a

	GARNET		BIOTITE		GARNET		STAU		GARNET		BIOTITE		STAUROLITE	
	core1	tran1	rim1		rim2	core2	rim2		rim	rim				
SiO2	35.651	36.482	37.034	33.285	32.657	36.781	37.328	36.494	26.717	36.573	35.224	31.102	26.73	
TiO2	0.046	0.057	0	1.48	1.55	0	0.039	0.009	0.49	0.137	0.003	1.016	0.737	
Al2O3	21.121	22.007	21.785	18.758	18.801	21.827	21.678	21.826	54.349	19.055	18.569	16.717	47.037	
FeO	31.732	32.922	32.593	18.724	18.595	33.333	31.986	32.364	14.393	34.44	34.655	22.775	15.423	
MnO	5.676	5.659	5.659	0.173	0.176	5.48	6.428	5.916	0.207	3.766	3.731	0.168	0.274	
MgO	2.85	2.257	2.625	9.317	9.422	2.508	2.879	2.511	1.859	1.902	2.275	7.737	1.002	
CaO	1.786	1.609	1.405	0.183	0.309	1.454	1.854	1.273	0.147	1.734	1.275	0.348	0.004	
Na2O	0.087	0	0.001	0.389	0.167	0.01	0.254	0	0.004	0	2.334	0.385	0	
K2O	0	0.14	0	8.469	8.305	0	0	0	0	0	0.217	6.589	0	
TOTAL	98.949	101.13	101.1	90.778	89.982	101.39	102.45	100.39	98.166	97.607	98.283	86.837	91.207	
Si	2.9239	2.9289	2.9615	2.6602	2.6331	2.9428	2.9514	0.0113	7.7522	3.0534	2.9643	2.6528	8.4202	
Ti	0.0028	0.0034	0	0.089	0.094	0	0.0023	2E-06	0.1069	0.0086	0.0002	0.0652	0.1746	
Al	2.0422	2.0829	2.0538	1.7674	1.7872	2.0588	2.0207	7.9772	18.592	1.8755	1.8423	1.681	17.468	
Fe2+	2.1766	2.2105	2.1798	1.2515	1.2539	2.2304	2.1151	0.0084	3.4927	2.4047	2.4391	1.6246	4.0632	
Mn	0.3943	0.3848	0.3833	0.0117	0.012	0.3714	0.4305	0.0016	0.0509	0.2663	0.266	0.0121	0.0731	
Mg	0.3484	0.27	0.3128	1.1097	1.1322	0.299	0.3393	0.0012	0.8039	0.2367	0.2853	0.9835	0.4704	
Ca	0.157	0.1384	0.1204	0.0157	0.0267	0.1246	0.1571	0.0004	0.0457	0.1551	0.115	0.0318	0.0014	
Na	0.0138	0	0.0002	0.0603	0.0261	0.0016	0.0389	0	0.0023	0	0.3809	0.0637	0	
K	0	0.0143	0	0.8635	0.8543	0	0	0	0	0	0.0233	0.717	0	
TOTAL	8.059	8.0334	8.0117	7.829	7.8195	8.0286	8.0554	8.0001	30.846	8.0003	8.3164	7.8318	30.671	

Selected probe data for samples 105 and 106b

	GARNET				GARNET			GARNET			STAUROLITE	BIOTITE				
	rim1	tran1	core1	tran1	rim1	tran2	core2	rim3	rim3	tran3			core3			
SiO2	36.158	36.768	36.816	36.727	37.06	36.544	36.281	36.635	36.675	36.912	36.497	37.15	26.467	26.353	34.373	34.743
TiO2	0.014	0.174	0	0	0	0.062	0.078	0	0.086	0.263	0.03	0.027	0.433	0.292	1.859	2.514
Al2O3	21.585	21.78	21.475	21.667	22.002	21.137	20.902	21.321	21.811	21.799	21.802	21.547	47.219	48.485	20.126	21.603
FeO	36.655	34.153	35.8	34.396	36.718	33.954	34.486	36.338	36.374	36.824	35.826	35.589	14.728	14.248	19.998	18.967
MnO	2.009	4.436	3.472	3.772	2.124	5.073	3.52	1.796	2.08	2.162	2.381	3.143	0.03	0.309	0.122	0
MgO	2.525	2.536	2.274	2.226	2.508	1.767	1.832	2.233	2.636	2.12	2.527	2.155	1.147	1.219	8.087	7.023
CaO	1.532	2.208	1.887	2.271	1.801	2.287	2.27	1.811	1.672	1.58	1.866	2.356	0.116	0.125	0.082	0.171
Na2O	0	0.272	0	0.123	0.191	0	0	0	0	0	0.33	0.208	0	0.356	0.107	0
K2O	0	0	0	0	0	0	0.021	0	0	0	0	0	0.376	0	8.689	8.019
TOTAL	100.48	102.33	101.72	101.18	102.4	100.82	99.39	100.13	101.33	101.66	101.26	102.18	90.516	91.387	93.443	93.04
Si2+	2.9264	2.9211	2.9472	2.946	2.9376	2.9563	2.969	2.9673	2.9349	2.9481	2.9264	2.9561	8.3854	8.2482	2.6674	2.6707
Tl 2+	0.0009	0.0104	0	0	0	0.0038	0.0048	0	0.0052	0.0158	0.0018	0.0016	0.1032	0.0687	0.1085	0.1453
Al 3+	2.0595	2.04	2.0267	2.049	2.0561	2.0159	2.0165	2.0359	2.0577	2.0525	2.0609	2.0213	17.637	17.891	1.8413	1.9578
Fe 2+	2.4811	2.2693	2.3968	2.3074	2.4341	2.2972	2.3602	2.4615	2.4344	2.4597	2.4025	2.3684	3.9025	3.7296	1.2979	1.2194
Mn 2+	0.1377	0.2985	0.2354	0.2563	0.1426	0.3476	0.244	0.1232	0.141	0.1463	0.1617	0.2118	0.0081	0.0819	0.008	0
Mg 2+	0.3046	0.3003	0.2713	0.2661	0.2963	0.213	0.2234	0.2695	0.3144	0.2523	0.302	0.2556	0.5416	0.5686	0.9353	0.8046
Ca 2+	0.1329	0.188	0.1619	0.1952	0.153	0.1982	0.199	0.1572	0.1434	0.1352	0.1603	0.2009	0.0394	0.0419	0.0068	0.0141
Na 2+	0	0.0419	0	0.0191	0.0294	0	0	0	0	0	0.0513	0.0321	0	0.2161	0.0161	0
K 2+	0	0	0	0	0	0	0.0022	0	0	0	0	0	0.152	0	0.8603	0.7864
total	8.043	8.0694	8.0394	8.0391	8.049	8.032	8.0191	8.0147	8.031	8.0099	8.0669	8.0477	30.769	30.846	7.7416	7.5983

Selected probe data for sample 106a

	GARNET				GARNET					STAUROLITE								BIOTITE
	core4	tran4	rim4	rim4	rim5	tran5	core5	tran5	rim5	rim	rim	rim	rim	rim	rim	rim	rim	
SiO2	35.722	36.219	35.737	34.988	35.792	36.032	35.534	35.88	35.898	26.174	26.349	33.462	26.554	26.283	26.394	26.932	33.813	33.462
TiO2	0	0.089	0	0	0.1	0	0.143	0.021	0.13	0.76	0.517	1.947	0.509	0.687	0.376	0.515	1.671	1.947
Al2O3	21.035	21.469	21.045	20.476	21.051	21.375	20.634	21.136	21.189	51.571	52.459	19.165	50.834	53.066	52.325	52.701	19.368	19.165
FeO	33.216	33.447	33.22	34.262	33.718	32.792	32.023	32.818	33.491	14.356	13.397	18.701	13.029	13.83	14.78	14.138	18.683	18.701
MnO	4.554	4.269	4.198	4.107	4.542	4.218	4.319	4.335	4.765	0.251	0.479	0.036	0.321	0.389	0.414	0.418	0.012	0.036
MgO	2.521	2.865	2.251	2.261	2.396	2.45	2.448	2.519	2.012	1.471	1.178	8.664	1.07	1.184	1.223	1.337	9.342	8.664
CaO	1.551	1.196	1.459	1.483	1.47	1.619	1.892	1.529	1.484	0.095	0	0.21	0	0.154	0.031	0	0.098	0.21
Na2O	0	0.188	0.188	0.009	0	0	0	0	0	0.087	0	0.129	0.019	0	0.007	0	0.17	0.129
K2O	0.055	0	0	0	0	0.059	0.044	0	0	0	0	8.495	0	0	0	0	8.691	8.495
TOTAL	98.654	99.742	98.098	97.586	99.069	98.545	97.037	98.238	98.969	94.765	94.379	90.809	92.336	95.593	95.55	96.041	91.848	90.809
Si	2.9414	2.9395	2.9549	2.9302	2.9387	2.9558	2.9629	2.9555	2.9486	7.8874	7.924	11.631	8.1418	7.823	7.8956	7.9796	2.6613	2.6654
Ti	0	0.0054	0	0	0.0062	0	0.009	0.0013	0.008	0.1722	0.1169	0.509	0.1174	0.1538	0.0846	0.1148	0.0989	0.1166
Al	2.042	2.0541	2.0515	2.0217	2.0377	2.0672	2.0284	2.0525	2.0518	18.321	18.599	7.8534	18.375	18.621	18.453	18.408	1.7971	1.7997
Fe 2+	2.2874	2.2702	2.2972	2.3997	2.3153	2.2497	2.2331	2.2608	2.3006	3.618	3.3695	5.4363	3.341	3.4427	3.6977	3.5033	1.2298	1.2458
Mn	0.3176	0.2935	0.294	0.2913	0.3159	0.2931	0.305	0.3025	0.3315	0.0641	0.122	0.0106	0.0834	0.0981	0.1049	0.1049	0.0008	0.0024
Mg	0.3094	0.3465	0.2774	0.2822	0.2932	0.2995	0.3042	0.3092	0.2463	0.6606	0.528	4.4881	0.4889	0.5252	0.5452	0.5904	1.0958	1.0285
Ca	0.1368	0.104	0.1293	0.1331	0.1293	0.1423	0.169	0.135	0.1306	0.0307	0	0.0782	0	0.0491	0.0099	0	0.0083	0.0179
Na	0	0.0296	0.0301	0.0015	0	0	0	0	0	0.0508	0	0.0869	0.0113	0	0.0041	0	0.0259	0.0199
K	0.0058	0	0	0	0	0.0062	0.0047	0	0	0	0	3.7671	0	0	0	0	0.8727	0.8633
TOTAL	8.0405	8.0428	8.0344	8.0597	8.0363	8.0137	8.0163	8.0169	8.0175	30.805	30.66	33.86	30.559	30.713	30.795	30.701	7.7906	7.7597

Selected probe data for sample 105e

	GARNET						GARNET						GARNET						
	rim1	tran1	core1	tran1	rim1	rim2	tran2	core2	tran2	rim2	rim3	tran3	core3	tran3	rim3	tran4	rim4	tran4	
SiO2	35.697	35.225	35.929	35.903	35.713	35.686	35.48	35.805	35.635	35.601	35.845	36.508	36.009	35.926	36.358	36.182	35.697	36.114	
TiO2	0	0	0	0.091	0.027	0	0.117	0.067	0	0	0.038	0.078	0.167	0.052	0	0.054	0.222	0.133	
Al2O3	20.249	20.576	20.654	20.691	20.554	20.772	20.429	20.069	20.96	20.443	20.831	21.611	21.332	21.198	21.384	22.008	21.039	21.622	
FeO	33.745	33.057	32.813	32.161	32.824	32.681	32.725	33.107	33.554	33.092	33.831	33.155	32.558	32.626	32.893	32.818	32.542	33.365	
MnO	4.299	3.943	4.424	3.967	4.449	4.372	3.851	3.949	4.196	4.517	4.899	4.538	4.696	4.978	4.67	4.853	4.733	4.295	
MgO	2.112	2.326	2.524	2.41	2.226	2.214	2.272	2.292	2.327	2.06	2.482	2.872	2.568	2.581	2.319	2.16	2.008	2.628	
CaO	1.471	1.572	1.63	1.676	1.528	1.384	1.688	1.733	1.586	1.443	1.459	1.387	1.428	1.716	1.54	1.435	1.612	1.271	
Na2O	0.125	0	0.179	0	0.193	0.178	0	0.031	0.161	0	0	0	0	0.077	0	0.046	0.077	0.309	
K2O	0	0	0	0	0	0	0	0	0	0.013	0.41	0	0	0	0.005	0	0	0	
TOTAL	97.698	96.699	98.153	96.899	97.176	97.514	97.287	96.562	97.053	98.419	97.169	99.795	100.15	98.758	99.154	99.169	99.556	97.93	99.737
Si	2.9766	2.9565	2.9682	2.9882	2.9825	2.9724	2.9719	2.9755	2.9934	2.9435	2.9775	2.9351	2.9464	2.9392	2.9659	2.9392	2.9552	2.9324	
Ti	0	0	0	0.0057	0.0038	0.0017	0	0.0074	0.0042	0	0	0.0023	0.0047	0.0103	0.0032	0	0.0138	0.0081	
Al	1.9906	2.036	2.0116	2.0303	2.0499	2.0168	2.0394	2.0198	1.978	2.0411	2.0157	2.0109	2.0562	2.0592	2.0445	2.1077	2.0534	2.0698	
Fe2+	2.3533	2.3204	2.2671	2.2387	2.2809	2.2848	2.2762	2.2953	2.3148	2.318	2.3147	2.3168	2.2378	2.2295	2.2323	2.244	2.2296	2.2658	
Mn	0.3036	0.2803	0.3096	0.2797	0.3142	0.3137	0.3084	0.2736	0.2797	0.2936	0.32	0.3398	0.3102	0.3257	0.345	0.3227	0.3339	0.3319	
Mg	0.2625	0.2909	0.3108	0.2989	0.2322	0.2761	0.2748	0.284	0.2856	0.2865	0.2568	0.3029	0.3454	0.3134	0.3147	0.2819	0.2615	0.2477	
Ca	0.1314	0.1414	0.1443	0.1495	0.1254	0.1363	0.1235	0.1517	0.1552	0.1404	0.1293	0.128	0.1199	0.1253	0.1504	0.1346	0.1249	0.143	
Na	0.0202	0	0.0287	0	0.0311	0.0287	0	0.005	0.0258	0	0	0	0	0.0122	0	0.0072	0.0124	0.0487	
K	0	0	0	0	0	0	0	0	0	0.0014	0.0428	0	0	0	0.0005	0	0	0	
TOTAL	8.0382	8.0255	8.0403	7.9909	7.9888	8.033	8.0228	8.0072	8.0159	8.0488	8.0153	8.0786	8.0208	8.0117	8.0415	8.0061	8.0073	8.0105	8.0489

Selected probe data for sample 105e

	SAMPLE 104a			SAMPLE 104b							
	BIOTITE	STAUROLITE		MUSC.	GARNET	STAUROLITE		BIOTITE			
		rim	core	rim		rim	rim				
SiO2	34.359	36.495	27.042	27.287	27.866	26.717	44.573	36.505	27.333	27.212	35.475
TiO2	2.425	1.166	0.5	0.502	0.653	0.49	0.591	0.05	0.644	0.515	1.76
Al2O3	18.685	21.415	53.837	54.243	54.303	54.349	34.101	21.537	53.545	53.561	19.529
FeO	19.671	17.599	13.929	13.892	12.847	14.393	1.088	30.623	13.852	12.268	16.653
MnO	0.189	0.219	0.819	0.648	0.561	0.207	0	7.378	0.711	0.682	0.302
MgO	9.156	9.371	1.662	2.063	1.441	1.859	0.796	2.558	2.088	1.814	9.584
CaO	0.225	0.143	0.001	0	0.076	0.147	0.228	1.759	0	0.077	0.123
Na2O	0	0	0.293	0.355	0.308	0.004	0.859	0.152	0.163	0	0.299
K2O	8.017	7.825	0	0	0	0	8.034	0	0	0.44	8.286
total	92.727	94.233	94.233	98.99	98.055	98.166	90.27	100.56	98.336	96.569	92.011
Si	2.6801	2.7378	7.8598	7.8506	8.0339	7.7522	3.0907	2.9425	7.914	7.9732	2.7422
Ti	0.1423	0.0658	0.1093	0.1086	0.1416	0.1069	0.0308	0.003	0.1402	0.1135	0.1023
Al	1.7183	1.894	18.448	18.398	18.457	18.592	2.7877	2.0466	18.277	18.502	1.7797
Fe 2+	1.2833	1.1042	3.3859	3.3426	3.0976	3.4927	0.0631	2.0643	3.3543	3.0062	1.0766
Mn	0.0125	0.0139	0.2016	0.1579	0.137	0.0509	0	0.5037	0.1744	0.1693	0.0198
Mg	1.0644	1.0477	0.7199	0.8846	0.6192	0.8039	0.0823	0.3073	0.901	0.7921	1.1041
Ca	0.0188	0.0115	0.0003	0	0.0235	0.0457	0.0169	0.1519	0	0.0242	0.0102
Na	0	0	0.1651	0.198	0.1722	0.0023	0.1155	0.0238	0.0915	0	0.0448
K	0.7978	0.7489	0	0	0	0	0.7107	0	0	0.1645	0.8171
total	7.7174	7.6238	30.89	30.941	30.682	30.846	6.8977	8.0431	30.853	30.745	7.6967

Selected probe data for samples 104a and 104b

APPENDIX D

1. Sample Preparation for XRF:

The method of preparation is as follows;

- a. Weathered surfaces were removed from the rock prior to crushing in the jaw crusher.
- b. The crushed sample was then milled in a tungsten carbide mill for 45->60 seconds, depending on the samples mica content.
- c. Approximately 2 grams of milled powder was ignited to 960 degrees for 12 hours to determine percentage loss of volatiles.
- d. Approximately 1 gram of ignited powder was weighed out with approximately 4 grams of flux. This mixture was fused into discs for whole rock analysis using X.R.F. techniques.
- e. Approximately 5 grams of unignited rock powder was mixed with 0.7ml of P.V.A. solution and made into pressed pellets, using boric acid as a support medium, for trace element determination.

2. Analytical Method

Whole rock analyses were determined by X-ray fluorescence

Major Elements

The following major elements were analysed for using a programmable Phillips PW 1480 X-ray spectrometer: SiO₂, Al₂O₃, Fe₂O₃, MnO, CaO, Na₂O, K₂O, TiO₂, P₂O₅ and SO₃.

Trace Element Analysis

The following trace elements were analysed for using a programmable Phillips PW 1480 X-ray spectrometer; Y, Sr, Nb, Zr, Pb, U, Ga, Zn, Ba, Sc, Cr, V, Co, Ce, Nd, La, Cu and Ni.

3. Results

A number of samples give low results, this can be attributed to the presence of H₂O and OH in the minerals, ie. the proportion of these components in staurolite is not certain. Thus the samples with significant modal abundances of staurolite ie.107b, may have low bulk chemical totals.

NEW BULK 4/11

	104a	104b	104c	104d	105i	105ii	105e	105w	106a	106b
SiO2	61.91	57.07	61.59	62.2	66.42	64.17	62.91	62.66	56.69	61.67
Al2O3	17.96	17.17	17.2	18.92	16.44	16.97	13.23	18.35	14.85	15.98
FeO	6.89	7.46	8.46	7.72	7.35	8.18	11.21	8.95	16.08	10.24
MnO	0.07	0.08	0.1	0.08	0.12	0.11	0.18	0.11	0.5	0.09
MgO	3.43	3.45	3.7	3.12	2.72	2.89	4.61	3.05	3.24	3.54
CaO	1.05	0.66	0.42	0.42	0.21	0.24	0.24	0.25	0.52	0.21
Na2O	1.38	0.83	0.51	0.38	0.17	0.2	0.15	0.19	0.34	0.18
K2O	3.64	3.67	3.82	3.2	2.63	3.05	3.6	3.16	3.23	3.46
TiO2	0.76	0.77	0.77	0.84	0.71	0.77	0.63	0.84	0.63	0.75
P2O5	0.15	0.14	0.15	0.018	0.13	0.16	0.13	0.17	0.1	0.14
SO3	0	0	0	0	0	0	0	0	0.01	0
LOI	1.65	1.69	1.47	1.78	1.68	1.6	1.76	1.11	2.36	1.35
TOTAL%	98.89	92.99	98.19	98.68	98.58	98.34	98.65	98.84	98.55	97.61
Y	30.5	33.1	15.9	29.9	27.7	30	34.6	32.2	33.5	30.3
Sr	111.8	74.6	38.7	24.5	15.6	16.5	9	14.3	78.3	17.3
Rb	177.4	182.2	185.6	166.6	122.7	138.6	189.2	152.4	192.6	175.3
Nb	15.6	17.1	16.1	16.6	11.4	13.9	14.2	15	15.2	15.2
Zr	143.8	147.7	170.8	172.8	137	175.8	150	192.6	136.6	167.8
Th	15.1	15.8	15.2	17.4	14.6	16.3	11.1	16.6	14.1	17
Pb	5.1	3.5	0.3	2.6	1.8	2	2.1	1.5	3.3	1
U	1.7	1.4	5.2	3.8	3.1	2.9	3.8	4.2	2	5.7
Ga	28	29.4	27.8	31.7	26.9	26.7	19.5	28.3	24	27.2
Cu	3	2	1	29	41	48	55	52	274	70
Zn	45	53	60	75	89	75	34	93	47	63
Ni	64	66	61	58	45	43	61	51	25	56
Ba	969	969	1112	1089	842	1091	723	1163	913	997
Sc	18.8	19.9	18	22.4	15.9	17.5	11.1	20.3	10.6	18.5
V	132.2	139.8	130	150.1	113.2	121.7	101.4	139.1	122	127.2
Co	35.8	31.9	39.4	41.4	48.6	48.4	48.2	36.1	17	41.1
Ce	64	72	25	63	80	62	50	77	68	67
Nd	27	29	7	28	29	26	18	33	16	27
La	30	31	10	32	35	30	21	38	26	28

NEW BULK 4/11

	107a	107b	107c	108	108 s	109	110	111
SiO2	61.61	49.95	62.14	58.05	58.19	58.5	59.19	58.71
Al2O3	13.11	12.33	12.67	16.73	19.64	16.79	18.92	19.37
FeO	14.37	20.80	14.20	11.29	11.63	11.14	10.02	9.86
MnO	0.4	0.26	0.41	0.09	0.1	0.09	0.12	0.11
MgO	2.73	2.39	3.32	3.69	3.58	3.61	3.47	3.64
CaO	0.38	0.22	0.36	0.27	0.21	0.27	0.25	0.21
Na2O	0.19	0.13	0.14	0.34	0.25	0.33	0.28	0.29
K2O	2.82	2.42	3.03	3.53	3.36	3.47	3.72	4.12
TiO2	0.46	0.45	0.49	0.76	0.79	0.76	0.76	0.79
P2O5	0.1	0.3	0.09	0.07	0.09	0.07	0.14	0.14
SO3	0.02	0.03	0.02	0	0	0	0	0
LOI	2.7	4.13	2.17	1.38	1.14	1.19	1.25	1.31
TOTAL%	98.89	93.41	99.04	96.20	98.98	96.22	98.12	98.55
Y	30.2	20.5	23.7	25.9	27.7	28.8	29.4	28.4
Sr	61.8	88.4	72.7	74.5	66.6	18.4	20.8	18.8
Rb	148.2	141.1	164.4	195.6	179.7	177.2	178.2	182.7
Nb	11.5	10.9	12.7	17.2	15.6	16.5	15.7	16.7
Zr	107.7	211.3	96.4	137.7	125.3	137.4	139.5	127.4
Th	8.8	10.6	10.1	16.5	17.2	16.9	15.7	15.5
Pb	3.1	4.3	3.2	5.5	0.2	6.2	0.4	1.2
U	2.2	8.9	4.5	3.6	2.9	5.3	3.5	3.8
Ga	22.9	24.6	19.6	28.4	31.3	26.9		28.4
Cu	260	703	203	93	146	62	27.3	41
Zn	53	85	29	95	112	100	56	72
Ni	17	22	19	57	53	60	83	64
Ba	703	597	820	914	900	862	1229	1353
Sc	8.1	9.9	10.8	19.2	21	19.2	19.4	20.1
V	86.8	141.1	110.2	137	143.5	139.5	145.1	145
Co	19.5	32	29	29.5	35.5	24.8	30	25.9
Ce	61	62	62	85	89	86	71	59
Nd	18	14	18	33	33	32	29	22
La	26	27	28	40	43	40	32	25